Received: 23 February 2024 | Revised: 28 August 2024 | Accepted: 3 September 2024

DOI: 10.1002/hyp.15282

RESEARCH ARTICLE

WILEY

River corridor beads are important areas of floodplain-groundwater exchange within the Colorado River headwaters watershed

Evan Y. Schulz[1] | Ryan R. Morrison[1] | Ryan T. Bailey[1] | Muhammad Raffae[1] | Jeffrey G. Arnold[2] | Michael J. White[2]

[1]Department of Civil and Environmental Engineering, Colorado State University, Fort Collins, Colorado, USA

[2]Grassland Soil and Water Research Laboratory, USDA–ARS, Temple, Texas, USA

Correspondence
Ryan R. Morrison, Department of Civil and Environmental Engineering, Colorado State University, 1372 Campus Delivery, Fort Collins, CO, USA.
Email: ryan.morrison@colostate.edu

Funding information
U.S. Department of Agriculture; National Science Foundation, Grant/Award Numbers: 2115169, 2142761; Walton Family Foundation

Abstract

Floodplains are essential ecosystems that provide a variety of economic, hydrologic, and ecologic services. Within floodplains, surface water-groundwater exchange plays an important role in facilitating biogeochemical processes and can have a strong influence on stream hydrology through infiltration or discharge of water. These functions can be difficult to assess due to the heterogeneity of floodplains and monitoring constraints, so numerical models are useful tools to estimate fluxes, especially at large spatial extents. In this study, we use the SWAT+ (Soil and Water Assessment Tool) ecohydrological model to quantify magnitudes and spatiotemporal patterns of floodplain surface water-groundwater exchange in a mountainous watershed using an updated version of the *gwflow* module that directly calculates floodplain-aquifer exchange rates during periods of floodplain inundation. The *gwflow* module is a spatially distributed groundwater modelling subroutine within the SWAT+ code that uses a gridded network and physically based equations to predict groundwater storage, groundwater head, and groundwater fluxes. We used SWAT+ to model the 7516 km^2 Colorado River headwaters watershed and streamflow data from USGS gages for calibration and testing. Models that included floodplain-groundwater interactions outperformed those without such interactions and provided valuable information about floodplain exchange rates and volumes. Our analyses on the location of floodplain fluxes in the watershed also show that wider areas of floodplains, "beads" (e.g., like beads on a necklace), exchanged a higher net and per area volume of water, as well as higher rates of exchange, compared to narrower areas, "strings." Study results show that floodplain channel-groundwater exchange is a valuable process to include in hydrologic models, and model outputs could inform land conservation practises by indicating priority locations, such as beads, where substantial hydrologic exchange occurs.

KEYWORDS
beads, Colorado, floodplain, floodplain-groundwater exchange, *gwflow*, hydrologic connectivity, river corridor, SWAT+

1 | INTRODUCTION

1.1 | Surface water-groundwater interactions in floodplains

While there are numerous ways to define floodplains (Junk et al., 1989; Nanson & Croke, 1992), they are broadly defined as surfaces within a river corridor and adjacent to the channel that are periodically inundated by water (Wohl, 2021). Floodplains are some of the most biologically diverse and productive landscapes on Earth (Tockner & Stanford, 2002; Ward et al., 1999), and as such, can have significant economic (Costanza et al., 1997), ecologic (Opperman et al., 2010), and hydrologic (Ward et al., 2002) impacts that extend beyond their immediate vicinity. A foremost physical function of floodplains is the attenuation of water, sediment, and nutrients, which is impacted by hydrologic exchanges, floodplain spatial extent, and floodplain heterogeneity (Wohl, 2021). Floodplain heterogeneity can vary greatly, both locally and longitudinally along a river corridor. Wider, lower gradient segments of river corridors, which Stanford et al. (1996) described as "beads," are likely to have greater diversity of habitat and storage of organic materials than their counterpart, "strings," which are narrower, steeper segments (Wohl et al., 2017). An understanding of floodplain functions requires a study of both hydrologic processes and floodplain physical properties due to the large variations in these characteristics along a river corridor.

Surface water-groundwater exchanges are of particular interest when examining floodplain hydrologic processes. Interactions with the alluvial aquifer can strongly influence hydrologic dynamics on the floodplain surface and in the river channel (Helton et al., 2014; Tonina & Buffington, 2009). This can be especially important during extreme hydrologic conditions or pollutant loading, where groundwater infiltration and discharge mitigate impacts on the ecosystem (Brunke & Gonser, 1997). Furthermore, groundwater processes can exert a strong influence on nutrient concentrations, pollutant filtering, and riparian vegetation (Stanford & Ward, 1993), which has cascading impacts on riparian ecosystems (Boulton et al., 1998). Floodplains may also provide substantial groundwater recharge. For instance, Goodrich et al. (2004) estimated that ephemeral channels, which are periodically inundated like floodplains, contribute between 15% and 40% of overall basin recharge to an aquifer in southern Arizona. Since surface water and groundwater interactions are known to play important roles in hydrologic, ecologic, and biogeochemical processes, they should be included in any effort to understand floodplain function.

However, floodplain surface water-groundwater exchanges are often highly complex due to heterogeneous hydraulic gradients and soil hydraulic conductivities (Krause et al., 2007; Woessner, 2000). The magnitude and spatial distribution of groundwater processes are determined by local controls (Cartwright et al., 2019), and can often vary with time (Andersen, 2004). While field measurements provide insight into these processes, assessing groundwater interactions accurately can be difficult, and results can depend on hydrologic connectivity (Brunner et al., 2009; Martinet et al., 2009). These challenges, exacerbated by anthropogenic changes that can cause novel and transient groundwater conditions, especially in floodplains, impede our understanding of groundwater flow patterns and floodplain exchanges.

1.2 | Numerical models of floodplain-groundwater exchange

Numerical models are useful tools for understanding interactions in complex landscapes, such as floodplains or aquifers, or in watersheds where detailed data collection may be infeasible or inefficient. Many models can simulate hydrologic, erosional, and/or biogeochemical processes, and incorporating physically based equations improves simulation accuracy. Numerical models can also aid in analysing the potential impacts of changing climate or land use, by adjusting forcing variables to simulate hypothetical scenarios.

Interest in floodplain exchanges has spurred research in modelling procedures that couple surface water and groundwater processes. Efforts that include two-dimensional hydrodynamic models and floodplain subsurface flows allow for detailed analyses of complex flow patterns and aquifer response to floods but are often limited to reach-scale systems due to high computing requirements (Bates et al., 2000; Maier et al., 2017; Saksena & Merwade, 2017). This limits applicability for modelling longer river corridors or entire watersheds, which can be necessary to understand catchment-scale management impacts.

The Soil and Water Assessment Tool (SWAT) is a watershed-scale simulation model that accounts for water, nutrient, and sediment storage and transport in a watershed setting with multiple land use and management configurations, reservoirs, wetlands, aquifers, and channels (Arnold et al., 1998). SWAT utilizes a discretization scheme in which a watershed is subdivided into lumped areas of similar soil, slope, and land use called hydrologic response units (HRUs). Water, nutrient, and sediment masses predicted from HRUs are passed to channels and routed through the channel network of the watershed on a daily time step. Spatially lumped models typically require fewer input data and less calibration effort while performing as well or better than spatially distributed models (de Vente et al., 2013). Recently, Bieger et al. (2017) developed an updated version of the model, SWAT+, to better represent watershed processes using a more flexible hydrologic routing structure. The internal algorithms of SWAT+ are consistent with the original SWAT model, but the change in routing structure can provide a more realistic representation of hydrologic

connectivity in a watershed (Bieger et al., 2019). SWAT+ and SWAT are publicly available.

Several studies have been performed using a SWAT framework to model floodplain processes. For instance, Liechti et al. (2014) and Phiri et al. (2021) used a modified version of the SWAT reservoir unit to better model the attenuation of floods through floodplains. Sun et al. (2016, 2018) performed multiple studies on the utilisation of landscape units (LUs) to better represent hydrologic and nitrate processes at both floodplain and catchment scales by improving the model simulation of surface water-groundwater exchange. Rajib et al. (2020) used SWAT to calculate forcing variables for hydrodynamic models to map flood extents at a large scale. The versatility of the SWAT model and breadth of existing research is promising for further research using SWAT to model watershed-scale processes.

While previous studies confirm the applicability of SWAT for modelling floodplain processes at large spatial extents, they have not fully addressed the hydrologic interactions between surface water and groundwater in floodplains. The studies outlined above focus on surface water attenuation through floodplains, denitrification processes, or flood mapping. Integrating floodplain exchanges with groundwater is still necessary to better simulate watershed processes holistically. Floodplains do not exist without interactions with aquifers or rivers, and including these processes in a watershed model is essential for an accurate representation of these systems. Furthermore, the simple default groundwater models in SWAT and SWAT+ make several simplifying assumptions that may be unrealistic in floodplain systems. These include steady state flow to streams instead of flow based on hydraulic gradients; homogeneous aquifer properties; and distinct aquifers that do not exchange flow between adjacent units.

To better represent groundwater processes, Bailey et al. (2020) developed the *gwflow* module, a subroutine within the SWAT+ modelling code that uses a control volume approach to update groundwater storage and groundwater head for a network of grid cells using calculated or specified groundwater inflows and outflows. Inflows and outflows include groundwater lateral flow, recharge, groundwater evapotranspiration, canal seepage, tile drainages outflow, groundwater-channel exchange, and groundwater-lake exchange (Bailey et al., 2022). However, direct calculations of surface water-groundwater exchange in floodplains have not yet been included.

1.3 | Study objectives

In this study, we update the *gwflow* module of SWAT+ to compute channel-groundwater exchange within floodplains in a mountainous watershed in Colorado, USA. The updated module explicitly calculates floodplain-groundwater interactions during periods of simulated floodplain inundation. Our overall objective is to investigate the hydrologic impacts and locations of floodplain-groundwater exchanges at a watershed scale. The specific goals of this research include: (i) evaluating SWAT+ model performance with and without the inclusion of floodplain-groundwater interactions in the *gwflow* module, (ii) investigating hydrologic pathways and fluxes when the floodplain-groundwater interaction is included, and (iii) identifying the magnitude and location of floodplain-groundwater exchanges in the study watershed, specifically in the context of beads and strings.

2 | METHODS

2.1 | Description of study area

We applied SWAT+ with *gwflow* to the Colorado headwaters watershed, which is identified by the 8-digit hydrologic unit code (HUC8) 14010001 and located on the western face of the Rocky Mountains in Colorado (Figure 1). This 7516 km^2 watershed includes elevations from approximately 1750 to 4150 m. The Colorado headwaters watershed supplies water to regions on the eastern side of the Rocky Mountains, such as the Denver, Colorado area, through inter-basin transfers (Caldwell et al., 2012; Petsch Jr., 1985). It also contains the headwaters of the Colorado River, which is an important energy and municipal, agricultural, and industrial water source for roughly 40 million people (Andersen et al., 2007).

2.2 | Floodplain delineation

We selected the GFPLAIN algorithm (Knox et al., 2022; Nardi et al., 2019) to delineate hydrogeomorphic floodplain areas within the study watershed, to allow linkage between floodplain water and the aquifer within the hydrologic model. GFPLAIN implements terrain analysis techniques to extract the stream network from a digital terrain model. Each cell in the drainage network receives the maximum potential channel flow depth (h) for a recurrence interval i from the power law shown in Equation (1) using contributing upstream area (A) as a scaling parameter. In this equation, a and b are dimensionless scaling parameters which were 0.0035 and 0.36, respectively, for the study watershed based on previous work by Knox et al. (2022). In addition, the floodplain extent based on Knox et al. (2022) was delineated using a 30-m resolution DEM and had a recurrence interval of 100 years. We used a 10 km^2 contributing area threshold to initiate floodplain estimates (Knox et al., 2022), though Annis et al. (2019) and Nardi et al. (2018) have demonstrated that other recurrence interval floods and catchment thresholds can be targeted.

$$h_i = aA^b. \quad (1)$$

The GFPLAIN algorithm then returns a gridded floodplain layer by flagging low-lying cells along river corridors and identifies the floodplain extent as the boundary of those cells that have land surface elevations lower than the corresponding maximum channel flow level.

2.3 | Including floodplain-groundwater exchange in the *gwflow* module

The *gwflow* module replaces the original groundwater module of SWAT+, which used a set of aquifer objects to relay recharge water

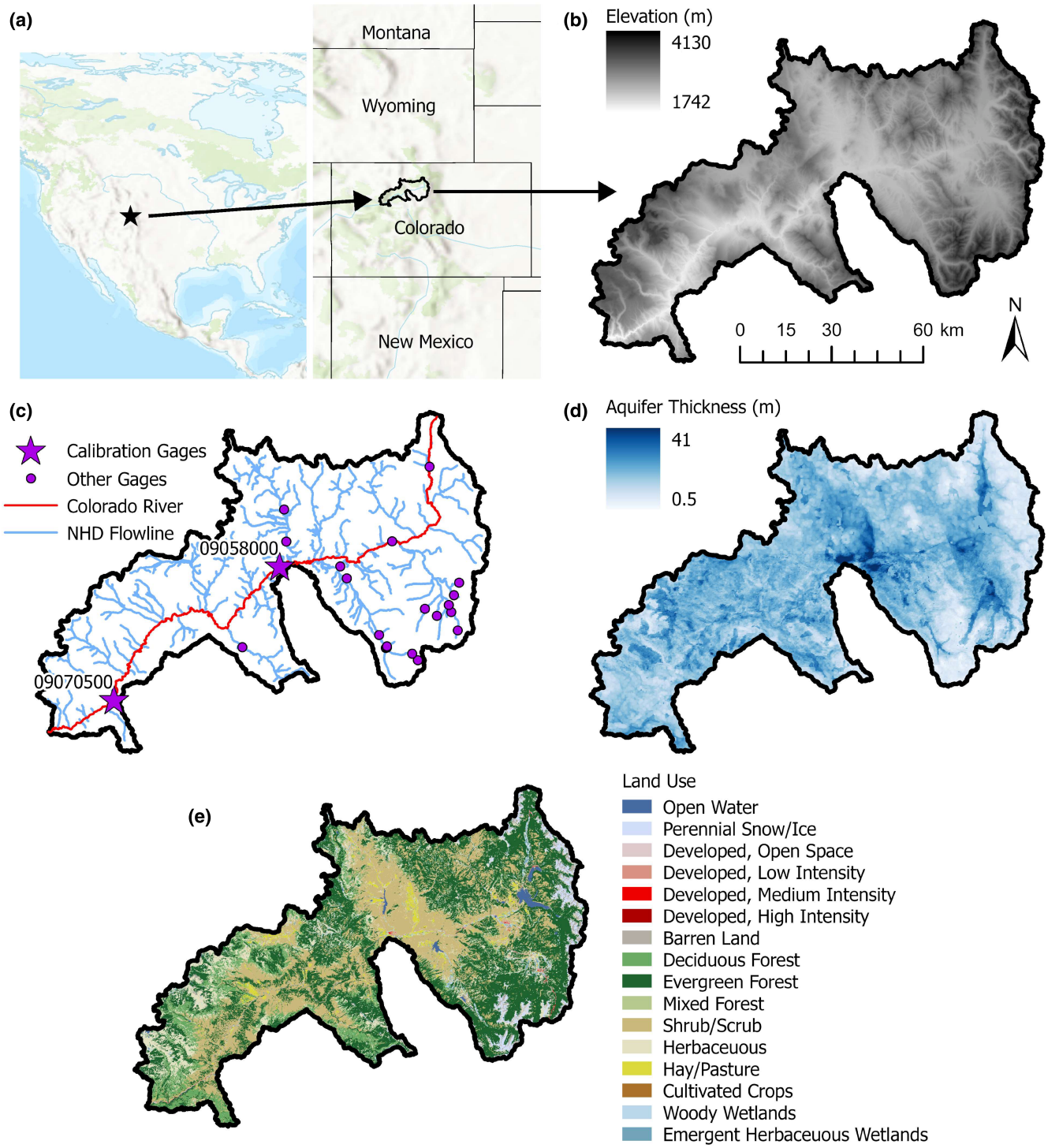

FIGURE 1 Location and properties of the Colorado Headwaters watershed, HUC8 14010001, showing: (a) vicinity map, (b) elevation range (Gesch et al., 2018), (c) USGS stream gages (U.S. Geological Survey, 2016), (d) aquifer thickness (Shangguan et al., 2017), and (e) land use (Dewitz, 2023).

to channels using linear routing equations. In contrast, the *gwflow* module uses a network of grid cells (Figure 2a) to track and update groundwater storage V (m^3), saturated thickness s (m), and groundwater head h (m) throughout the watershed's unconfined aquifer system, based on aquifer properties (hydraulic conductivity K, specific yield S_y) and a set of groundwater inflows and outflows. Each cell has unique values of K and S_y, and inflows and outflows change through time based on interactions with other hydrologic objects, such as HRUs, channels, reservoirs, wetlands, and canals. Updating V is performed for each grid cell, for each daily time step, using an explicit approach,

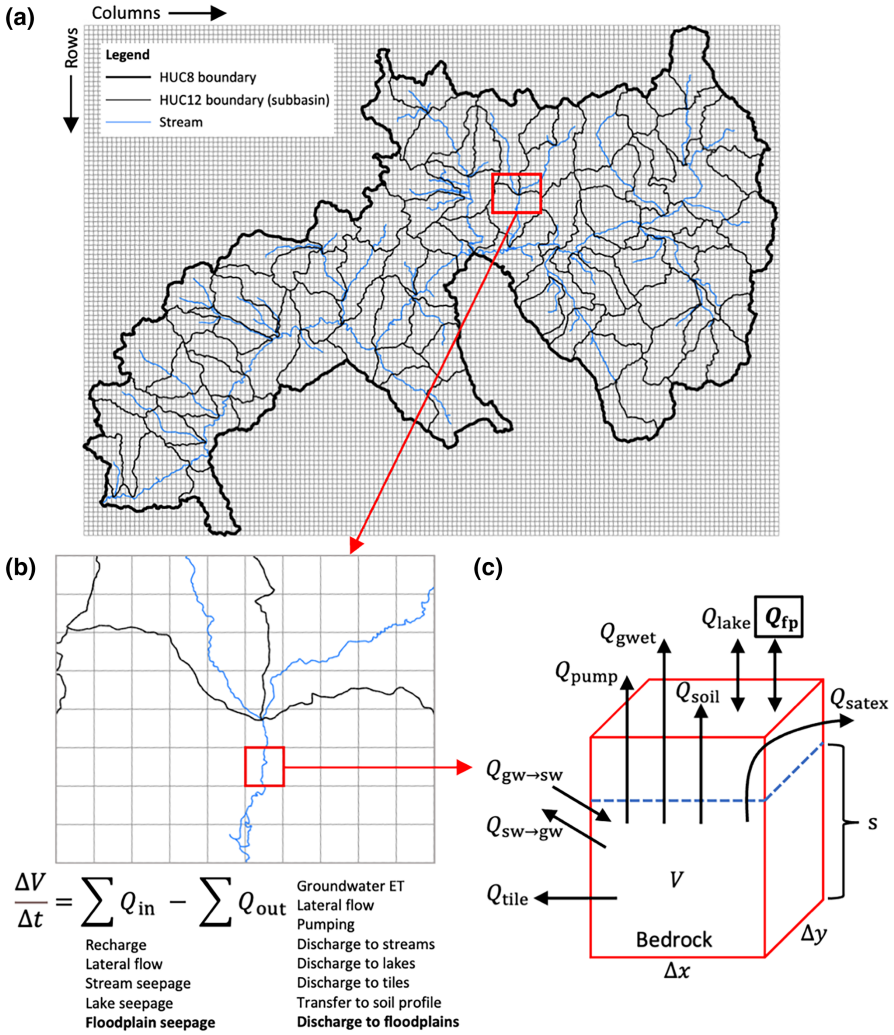

FIGURE 2 Layout and approach of the *gwflow* module where (a) shows the *gwflow* grid cell setup, (b) is a close-up of grid cells/streams with the general water balance equation used in *gwflow* calculations, and (c) is a conceptual schematic of the control volume approach for individual grid cells (after Bailey et al., 2023). The boxed term in (c) is a novel addition to the *gwflow* module for this study.

that is, a forward-in-time Euler method using cell values at time *i*. For a single grid cell, the change in storage *V* (Equation 2) and new storage *V* (Equation 3) at time $i + 1$ is calculated as:

$$\frac{\Delta V}{\Delta t} = \sum Q_{\text{inflows}} - \sum Q_{\text{outflows}}. \tag{2}$$

$$V_{i+1} = V_i + \left(\sum Q_{\text{inflows}} - \sum Q_{\text{outflows}}\right)(\Delta t), \tag{3}$$

where *Q* represents a daily flux rate (m^3/day); inflows include recharge, channel seepage, canal seepage, reservoir seepage, specified groundwater injection, and groundwater lateral inflow from surrounding cells; and outflows include groundwater evapotranspiration (ET), groundwater discharge to channels and reservoirs, pumping, saturation excess flow at the ground surface, tile drainage outflow, and groundwater lateral outflow to surrounding cells. Lateral flow between surrounding cells is computed using Darcy's Law, based on gradients of hydraulic head between the cells. These fluxes are also represented in Figure 2b,c. Once the new storage V_{i+1} is calculated, saturated thickness (m) and groundwater head (m) can be calculated for the cell using S_y. Table 1 provides a list of the groundwater inflows and outflows, how they are calculated, and how they connect to SWAT+ objects. Recharge volumes are transferred from HRUs to grid cells using geographic connection information (i.e., intersection polygons between HRUs and grid cells); groundwater-channel exchange occurs only for cells that intersect SWAT+ channels; and groundwater-reservoir exchange occurs only for cells that intersect SWAT+ reservoirs.

For our study, the groundwater storage calculation in Equation (2) is amended in the SWAT+ code to include groundwater-channel exchange in channel floodplains during periods of floodplain inundation, as simulated by the model. The updated *gwflow* module uses Equation (4) to calculate volumetric flow rates of floodplain exchange, where for each floodplain cell (notated by row *i* and column *j*), $Q_{\text{fp}\leftrightarrow\text{gw}\,i,j}$ is the channel-groundwater exchange rate (m^3/day), $A_{\text{fp}\,i,j}$ is the area over which exchange occurs (m^2), $K_{\text{fp}\,i,j}$ is the soil hydraulic conductivity (m/day) of the exchange area, $h_{\text{fp}\,i,j}$ is the channel water elevation (m), $h_{\text{gw}\,i,j}$ is groundwater head (m), and z_{fp} is the distance between the ground surface and groundwater head (m) (i.e., the

TABLE 1 Flux terms used in the *gwflow* module equations.

Flux in *gwflow*	Description	Connection to other SWAT+ hydrologic objects
Q_{rech}	Aquifer recharge	Provided to grid cells from HRU soil profile deep percolation. Uses spatial intersections between HRUs and grid cells.
$Q_{sw\rightarrow gw}$; $Q_{gw\rightarrow sw}$	Stream seepage to aquifer; Groundwater discharge to streams	Calculated using Darcy's Law for each grid cell that geographically intersects a stream channel. Discharge to streams is provided to the corresponding channel in SWAT+.
$Q_{lake\rightarrow gw}$; $Q_{gw\rightarrow lake}$	Lake seepage to aquifer; Groundwater discharge to lakes	Calculated using Darcy's Law for each grid cell that geographically intersects a lake or reservoir. Discharge to lakes is provided to the corresponding reservoir object in SWAT+.
Q_{gwet}	Groundwater evapotranspiration	Calculated using unsatisfied ET, i.e., remaining potential ET after actual ET has been calculated for HRU's soil profile.
$Q_{gw\rightarrow soil}$	Groundwater transfer to the soil profile	Provided to HRUs when groundwater levels rise above the bottom of the SWAT+ soil profile.
Q_{satex}	Saturation excess flow when the water table intersects the ground surface	Calculated when the water table rises above the ground surface. Fluxes are routed to the channel object to which the surface runoff of the corresponding HRU drains.
Q_{pump}	Groundwater pumping	Provided to HRUs when groundwater irrigation is specified. External demand can also be specified, with extracted groundwater volume then removed from the watershed system.
Q_{tile}	Groundwater discharge to tile drains	Calculated for grid cells that geographically include a tile drain. Fluxes are routed to the channel object to which the tile drains.
Q_{north}; Q_{south}; Q_{west}; Q_{east}	Groundwater lateral fluxes into/out of the four sides of each grid cell	Inflows to or outflows from adjacent grid cells. Calculated using Darcy's Law.
$Q_{fp\rightarrow gw}$; $Q_{gw\rightarrow fp}$	**Floodplain seepage to aquifer; Groundwater discharge to channels.**	**Calculated using Darcy's Law for each grid cell that geographically intersects a floodplain when channel flow is simulated to be in the floodplain.**

Note: Bolded text represents the new flux term for groundwater-channel water exchange in channel floodplains.

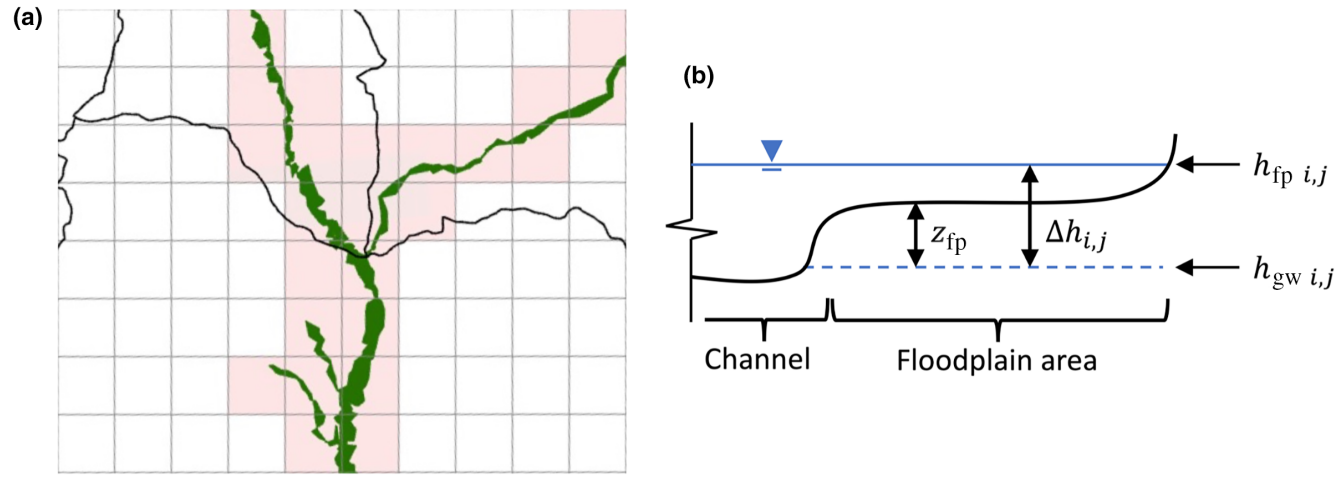

FIGURE 3 Schematic where (a) shows a close-up of grid cells (grey), the delineated floodplain (green), and floodplain cells (red), and (b) is a conceptual cross-section of a channel/floodplain area where surface water-groundwater exchange is calculated.

distance infiltrating water travels through soil). Figure 3b provides a conceptual diagram of the exchange calculation.

$$Q_{fp\leftrightarrow gw\,i,j} = A_{fp\,i,j}\,K_{fp\,i,j}\left(\frac{h_{fp\,i,j} - h_{gw\,i,j}}{z_{fp}}\right). \quad (4)$$

Channel-groundwater fluxes in floodplains can either recharge the aquifer from channel water, when channel stage is higher than groundwater head in the cell, or discharge groundwater to the floodplain, when groundwater head is higher than channel stage. Figure 3a shows an example of floodplain cells in a *gwflow* grid set up. Green polygons indicate the delineated floodplain, and red cells indicate cells ("floodplain cells") for which channel-groundwater exchange in the floodplain areas can be simulated. Exchange in these floodplain cells for a given day during the simulation period occurs only if floodplain inundation is simulated for the connected channel. The

TABLE 2 Datasets used for the construction of SWAT+ NAM models, *gwflow*, and *gwflow* with floodplain exchange (after Bailey et al., 2023).

	Dataset	Source	Data type/ resolution
SWAT+ model construction	Field boundaries	Yan and Roy (2016)	Raster/30 m
	Crop rotation	USDA-NASS, CDL	Raster/30 m
	Topographic slope	USGS National Elevation Dataset (Gesch et al., 2018)	Raster/10 m
	Soil boundaries and properties	Gridded Soil Survey Geographic (Soil Survey Staff, 2014)	Raster/10 m
	Land use, Land cover	U.S. Geological Survey, National Land Cover Data	Raster/30 m
	Stream segments	Moore and Dewald (2016)	Vector features/—
	Lakes and reservoirs	Moore and Dewald (2016)	Vector polygons/—
	Weather	Global historical climatology network; PRISM	—/HUC12
	Water use	Dieter et al. (2018)	—/HUC8
	Discharge from facilities	Skinner and Maupin (2019)	—/HUC12
gwflow module	Geologic units	Horton (2017)	Vector polygons/—
	Tile drainage	Valayamkunnath et al. (2020)	Raster/30 m
	Aquifer thickness	Shangguan et al. (2017)	Raster/250 m
	Groundwater head	U.S. Geological Survey (Bailey & Alderfer, 2022)	Vector points/—
gwflow (floodplain)	Floodplain delineation	Knox et al. (2022)	ESRI shapefile/30 m
	Floodplain hydraulic conductivity	Soil Survey Geographic Database (SSURGO) (Soil Survey Staff, 2011)	ESRI shapefile/—

floodplain exchange area A_{fp} for each floodplain cell is the overlap region between the cell and the floodplain, determined a priori using GIS intersection routines. If the cell also contains the main channel, then A_{fp} is decreased by the bed area of the main channel, as groundwater-channel exchange rates are also calculated for the cell.

SWAT+ assumes a trapezoidal channel defined by its bankfull width (width at the top of the channel), and a trapezoidal floodplain that has a bottom width equal to 5 times the channel bankfull width (Neitsch et al., 2009). The channel has sides with a 2:1 run to rise ratio while the floodplain has sides with a 4:1 run to rise ratio. When the volume of water routed to the channel exceeds its capacity, water inundates the floodplain. SWAT+ then calculates flow depth and volume as the sum of both channel and floodplain cross sections. Flow depth is used to establish h_{fp} in Equation (4).

The addition of floodplain exchanges requires a new *gwflow* input file, "gwflow.floodplain", which contains a list of cells that are within the floodplain. Each cell in the file list includes information for the area of intersection between the floodplain and the cell A_{fp}, a hydraulic conductivity value K_{fp}, and the ID of the connected channel within the SWAT+ model.

2.4 | SWAT+ model for the Colorado headwaters

The SWAT+ model used in this study encompasses the delineated 8-digit watershed shown in Figure 1 (HUC8 14010001). The model was derived from the National Agroecosystem Model (NAM) (Arnold et al., 2021; White et al., 2022), a collection of SWAT+ models that span the spatial extent of the conterminous United States, with one model for each 8-digit watershed. The models include delineations of cultivated fields, NHD+ channels, 12-digit catchments, soils, reservoirs and lakes, and wetlands. Table 2 outlines the datasets used in the development of NAM, to prepare inputs for the *gwflow* module, and to delineate the floodplain and populate floodplain K_{fp}.

2.5 | Model setup for floodplain exchange

The combined modelling system was tested with and without (control) floodplain exchange activated. The *gwflow* module setup procedure was identical for the control and floodplain scenarios except for the addition of the "gwflow.floodplain" input file in the floodplain scenario. The model simulation period was 1 January 2000 to 31 December 2015, which encompasses both wet and dry years in the study watershed based on years with streamflow above or below the long-term average discharge during the simulation period (see Supporting Information). For both scenarios, the *gwflow* module resolution used for analysis had uniform grid cells with 250 m sides. Aquifer zones (Figure 4a) were identified from a geologic map. The aquifer zones were consolidated from 9 to 5 zones to improve future calibration runtime after a preliminary calibration of 53 PEST (Doherty, 2018) procedures indicated that several zones had similar values for hydraulic conductivity and specific yield. Zones 1 (granite) and 9 (gravel) remained distinct while zones 2 (shale)/4 (n/a)/6 (sandstone), 3 (mafic-volcanic)/5 (arkose), and 7 (basalt)/8 (unconsolidated) were combined. Initial values and ranges for these consolidated zones were updated to account for the larger variability in geologic material.

We identified floodplain cells (Figure 4b; total of 12 357 floodplain cells) from an intersection of the *gwflow* grid and the GFPLAIN floodplain. This intersection also provided values of A_{fp} for each floodplain cell. We determined K_{fp} values from the Soil Survey Geographic (SSURGO) database (Soil Survey Staff, 2011). Due to the large number of saturated hydraulic conductivity (K_{sat}) values in the database, we

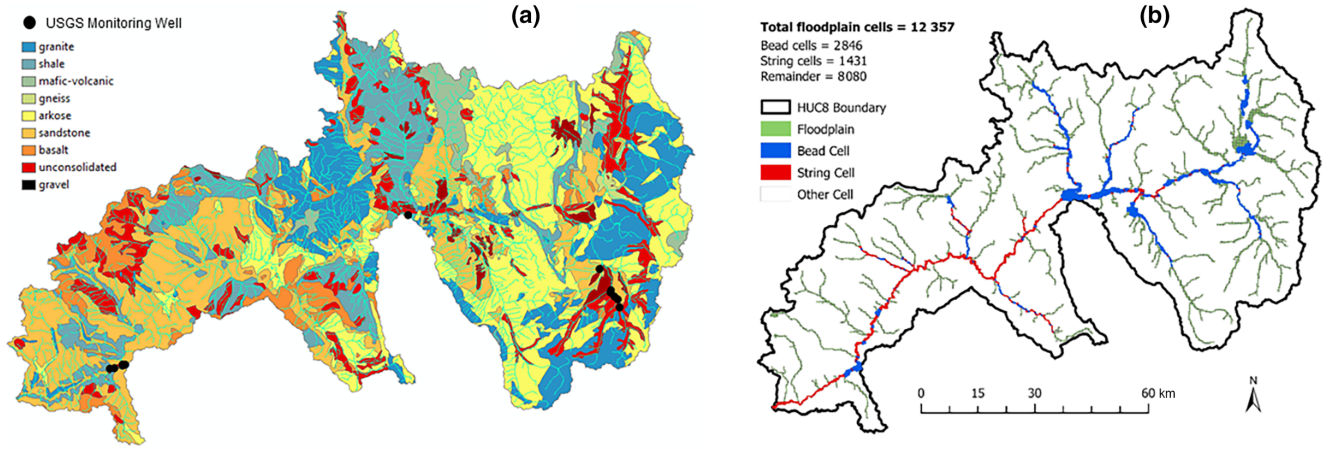

FIGURE 4 (a) Aquifer zone boundaries and locations of USGS monitoring wells; (b) Floodplain cells identified as beads (blue) or strings (red) using a 5-times median stream width threshold value. Note that "Other Cell" here refers to non-floodplain cells or floodplains of stream orders 1–3 where bead/string delineation was deemed inaccurate for the dataset resolution available for this study.

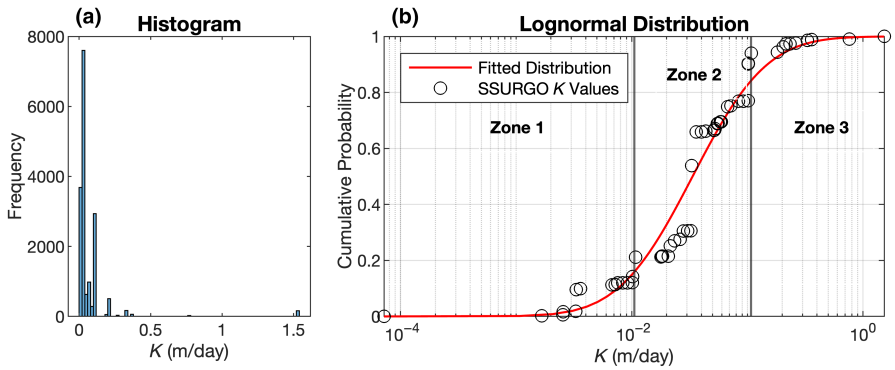

FIGURE 5 (a) Histogram and (b) fitted lognormal distribution for floodplain hydraulic conductivity K_{fp} zones.

used a histogram analysis (Figure 5) to consolidate the number of soil zones. We fit the values with a lognormal curve to delineate three zones of K_{sat}, and then assigned K_{fp} to each grid cell using the K_{sat} value from the zone that intersects the floodplain cell. Finally, we used the NHDPlus dataset (Moore & Dewald, 2016) to identify the closest channel ID to each floodplain cell.

To provide an analysis of floodplain exchange within beads and strings, we analysed the GFPLAIN floodplain shapefile to identify floodplain bead and string locations, and thereby bead and string cells. We used perpendicular transects generated from centerlines of the floodplain area to estimate floodplain width. For locations where the floodplain widths (transects) were above a threshold value for bead delineation, a flag identified that transect as the location of a bead. We analysed several threshold values based on median stream widths for individual stream orders to assess the sensitivity of results. Median stream widths were based on values from Downing et al. (2012) and the NHDPlus dataset (Moore & Dewald, 2016) defined stream orders and locations. The four threshold values were 3-, 5-, 7-, and 9-times median stream width. We describe this procedure in further detail in Supporting Information. For stream orders 1, 2, and 3, the threshold values for beads using the 5-times median stream width threshold were 8.0 m, 9.5 m, and 27.5 m, respectively. Since the resolution of the GFPLAIN shapefile is 30 m, we deemed identification of beads in these lower stream orders inaccurate. Thus, we constrained further analysis of beads and strings in the watershed to stream orders 4, 5, and 6, where 6 was the maximum stream order identified in the study area. The 5-times median stream width threshold values for stream orders 4, 5, and 6 were 55.0 m, 237.5 m, and 495.0 m, respectively. Figure 4b shows the result of intersecting *gwflow* floodplain cells with the closest transect to identify cells as representing a bead or string area. A total of 2846 and 1431 bead and strings cells, respectively, were identified, with a remainder of 8080 floodplain cells around stream orders 1–3 that were not included for further analysis.

2.6 | Model calibration and testing

We tested model results against monthly streamflow at two USGS gages (upstream gage: USGS 09058000, near Kremmling, CO; downstream gage: USGS 09070500, near Dotsero, CO) (Figure 1c) and groundwater head at a set of USGS monitoring wells (Figure 4a). For this comparison, we averaged daily simulated streamflow across each month. Other stream gages had limited contributing area or sparse

TABLE 3 Description, units, and final values of parameters included in the PEST model calibration.

Parameter	Description	Unit	Final (floodplain)	Final (control)
CN2 FRST A	Curve number–forest	–	20	15
CN2 FRST B	Curve number–forest	–	62	65
CN2 FRST C	Curve number–forest	–	57	43
CN2 FRST D	Curve number–forest	–	51	45
CN2 PAST A	Curve number–pasture	–	39	55
CN2 PAST B	Curve number–pasture	–	71	75
CN2 PAST C	Curve number–pasture	–	58	90
CN2 PAST D	Curve number–pasture	–	66	99
CN2 BRUSH A	Curve number–brush	–	27	53
CN2 BRUSH B	Curve number–brush	–	25	64
CN2 BRUSH C	Curve number–brush	–	62	45
CN2 BRUSH D	Curve number–brush	–	60	90
EPCO	Plant uptake factor	–	0.1	0.1
ESCO	Soil evaporation factor	–	0.1	0.1
PERCO	Percolation coefficient	–	1.0	0.9
CN3 SWF	Soil water factor for CN3	–	0.2	0.1
FALLTMP	Snowfall temperature	°C	5.0	5.0
MELTTMP	Snowmelt base temperature	°C	5.0	5.0
MELTMX	Melt factor for snow on June 21	mm H_2O/°C-day	3.4	3.4
MELTMN	Melt factor for snow on December 21	mm H_2O/°C-day	1.4	1.4
TIMP	Snowpack temperature lag factor	–	0.1	0.1
COVMX	Snow water content for 100% cover	mm H_2O	0.5	0.5
RECH_DEL	Recharge delay	day	6.0	3.2
$K_{aqu}1$	Aquifer *K* for Zone 1	m/day	7.19E−04	8.28E−04
$K_{aqu}2$	Aquifer *K* for Zone 2	m/day	1.00E−04	1.50E−04
$K_{aqu}3$	Aquifer *K* for Zone 3	m/day	2.23E−03	1.82E−03
$K_{aqu}4$	Aquifer *K* for Zone 4	m/day	6.10E+00	5.86E+00
$K_{aqu}5$	Aquifer *K* for Zone 5	m/day	1.03E+02	5.75E+01
S_y1	S_y for Zone 1	–	1.22E−01	1.35E−01
S_y2	S_y for Zone 2	–	6.79E−02	6.53E−02
S_y3	S_y for Zone 3	–	1.63E−01	3.48E−01
S_y4	S_y for Zone 4	–	3.94E−01	3.80E−01
S_y5	S_y for Zone 5	–	1.41E−01	1.08E−01
K_{stream}	*K* for stream bed	m/day	2.96E−07	3.36E−07
d_{stream}	Thickness of stream bed	m	1.18E−01	6.97E−02
$K_{fplain}1$	Floodplain *K* for Zone 1	m/day	5.88E−04	–
$K_{fplain}2$	Floodplain *K* for Zone 2	m/day	9.38E−02	–
$K_{fplain}3$	Floodplain *K* for Zone 3	m/day	3.90E−01	–

temporal data. We used PEST (Doherty, 2018) for model calibration, using a calibration period of 2003–2011 and a testing period of 2012–2015, with a 3-year warm up period of 2000–2002. We used a model with 1000 m *gwflow* cells to estimate model parameters, due to the long run times of the 250 m cell model. Parameters included in PEST (Table 3) cover a range of watershed processes such as land surface processes (runoff generation properties for forest, pasture, and brush; evapotranspiration properties; snowfall properties) and aquifer properties (*K*, S_y). K_{fp} values for each soil zone were included only in the floodplain scenario. We set initial ranges for all calibrated parameters based on reasonably expected values based on land and aquifer properties. Thus, we included 35 parameters in the control scenario and 38 parameters in the floodplain scenario. Resulting parameter values (Table 3) from the 1000 m cell model were used directly in the

250 m cell model. The 1000 m and 250 m models had cell parameters defined independently by intersecting their respective grids with aquifer and floodplain polygons. Calibrated values for each parameter were identical for each cell size. Parameter ranges and initial values are provided in Table S1. We ran all simulations on a desktop Intel® Core™ i7-7700 CPU @ 3.60 GHz, 64.0 GB RAM. The SWAT+ model runs using 250 m cells took roughly 150% longer to simulate than the equivalent 1000 m versions, for both floodplain and control scenarios. The control scenario completed calibration after ~484 h (~20 days) and the floodplain scenario completed calibration after ~528 h (~22 days). The control scenario converged after 31 optimization iterations and 2234 model runs, whereas the floodplain scenario converged after 42 optimization iterations and 2673 model runs.

We note an error in calibration regarding the curve number for the Forest and Brush land use types. As seen in Table 3, the CN B value for forest (65) is higher than the C and D values (43, 45); likewise, the CN B value for brush (64) is higher than the C value (45). Therefore, the runoff for the higher-infiltration soils is simulated as higher than the runoff for the lower-infiltration soils. This is an artefact of applying overlapping ranges of parameter values when applying PEST, whereas no overlapping should occur. Although runoff values for the B and C soil types likely are higher and lower, respectively, than in reality, surface runoff is approximately only 10% of generated streamflow in the basin (see Section 3.1.3). Therefore, although the CN values are not ideal, they do not affect the overall objective of investigating the impact of floodplains on basin hydrology.

Streamflow was assessed using Nash–Sutcliffe model efficiency coefficient (NSE) and Kling–Gupta efficiency (KGE), which measure model performance compared to the mean of observed time series data, and percent bias (PBIAS) and root-mean-square error (RMSE), which measures the tendency of the model to over- or underestimate values, as performance metrics. Equations (5)–(8) show the NSE, KGE, PBIAS, and RMSE calculations, respectively, where Q^i_{obs} is the i^{th} observed streamflow, Q^i_{sim} is the i^{th} simulated streamflow, $\overline{Q}_{obs}$ is the mean of observed streamflow, $\overline{Q}_{sim}$ is the mean of simulated streamflow, N is the total number of observations, r is the Pearson correlation coefficient (Equation 8), α is the ratio of standard deviations ($\sigma_{sim}/\sigma_{obs}$), and β is the ratio of means ($\overline{Q}_{sim}/\overline{Q}_{obs}$).

$$\mathrm{NSE} = 1 - \frac{\sum_{i=1}^{N}\left(Q^i_{obs} - Q^i_{sim}\right)^2}{\sum_{i=1}^{N}\left(Q^i_{obs} - \overline{Q}_{obs}\right)^2}. \quad (5)$$

$$\mathrm{KGE} = 1 - \sqrt{(r-1)^2 + (\alpha-1)^2 + (\beta-1)^2}. \quad (6)$$

$$\mathrm{PBIAS} = \frac{\sum_{i=1}^{N}\left(Q^i_{obs} - Q^i_{sim}\right)100}{\sum_{i=1}^{N}\left(Q^i_{obs}\right)}. \quad (7)$$

$$\mathrm{RMSE} = \sqrt{\frac{\sum_{i=1}^{N}\left(Q^i_{obs} - Q^i_{sim}\right)^2}{N}}. \quad (8)$$

$$r = \frac{\sum_{i=1}^{N}\left(Q^i_{obs} - \overline{Q}_{obs}\right)\left(Q^i_{sim} - \overline{Q}_{sim}\right)}{\sqrt{\sum_{i=1}^{N}\left(Q^i_{obs} - \overline{Q}_{obs}\right)^2}\sqrt{\sum_{i=1}^{N}\left(Q^i_{sim} - \overline{Q}_{sim}\right)^2}}. \quad (9)$$

Groundwater head was assessed using mean absolute percent error (MAPE) (Equation 10) to account for the relatively high simulated aquifer head due to watershed elevation. Of the 14 monitoring wells shown in Figure 4a, only 5 have more than 1 measurement value, and hence only those are included in our analysis.

$$\mathrm{MAPE} = \frac{100\%}{N}\sum_{i=1}^{N}\left|\frac{\mathrm{obs} - \mathrm{sim}}{\mathrm{obs}}\right|. \quad (10)$$

3 | RESULTS

3.1 | Model results and evaluation

3.1.1 | Floodplain delineation and simulation

The delineation of floodplains by the GFPLAIN algorithm (Figure 6a) resulted in 230 km^2 of floodplain area. As a qualitative comparison, our floodplain area tends to match the spatial distribution of lacustrine wetlands (Figure 6b), as mapped by the U.S. Fish and Wildlife Service (the total wetland area in the watershed is 343 km^2). Wetlands are not necessarily within floodplains, as wetlands can evolve due to areas of groundwater and soil saturation in other areas of the watershed (Fan et al., 2013); therefore, the smaller floodplain area is expected. Regarding the ability of the SWAT+ model to correctly simulate flooding (i.e., stream water is within the floodplain areas), Figure 6a shows the flood fraction, that is, the fraction of time during 2014 (as an example) that the channel is in the floodplain, for each of the 3077 channels in the model. Channels with a high (>20%) flood fraction tend to coincide spatially with locations of delineated floodplains and mapped wetlands. These results provide confidence that areas of water exchange between floodplains and the unconfined aquifer are established correctly within the model setup. The fraction of time during 2000–2015 that each *gwflow* cell is in connection with floodplain (Figure 6c) demonstrates that the floodplain-cell connection also is being implemented correctly. Of all the cells in connection with floodplains and that experience connection during the 2000–2015 period, 40% are in connection for more than 20% of the time, and 35% are in connection for more than 50% of the time (Figure 6d). Floodplain cells that exchange water with floodplains account for an area of 168 km^2, and those that exchange water for more than 20% of the time account for an area of 115 km^2. Approximately 1% of floodplain cells exchange water more than 95% of the time.

3.1.2 | Streamflow and groundwater head

Plots comparing simulated monthly streamflow with measurements and between scenarios (Figure 7) demonstrate that the model

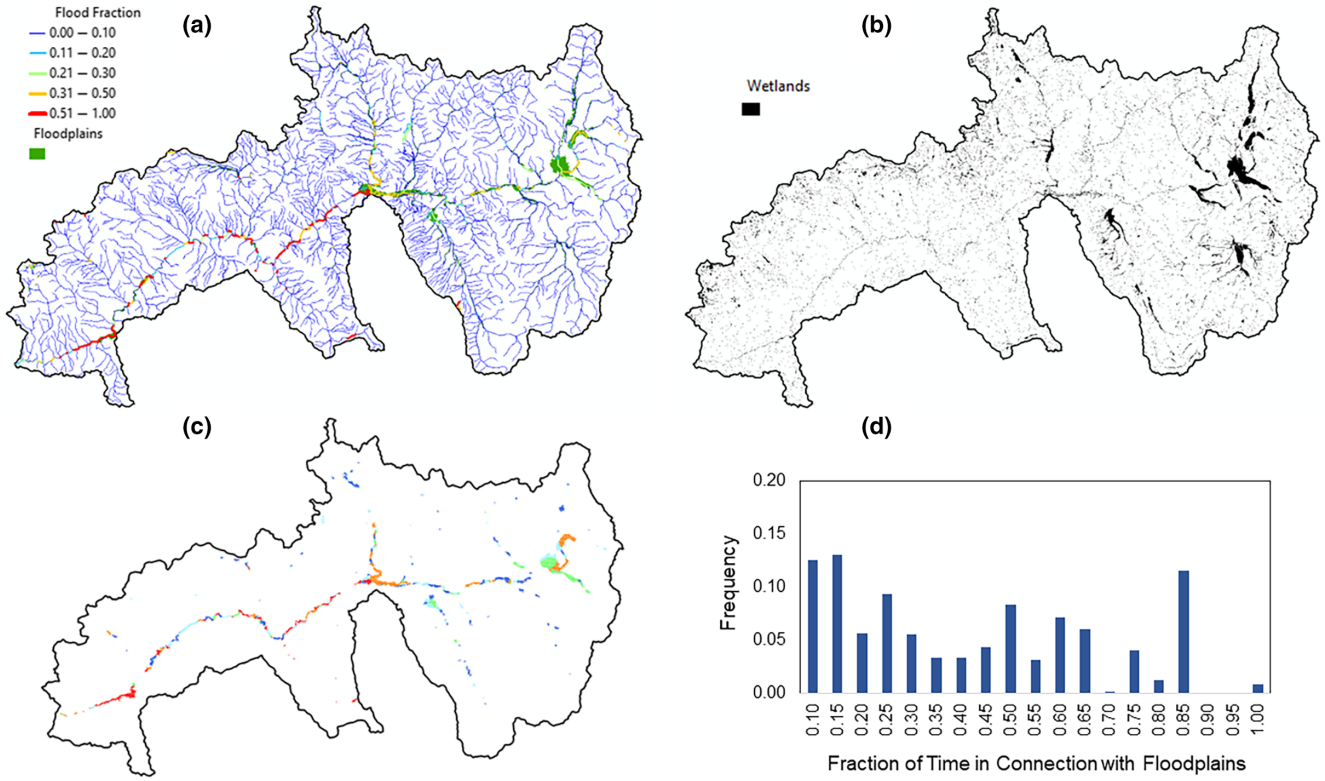

FIGURE 6 (a) Fraction of time during 2014 that water inundates a portion of the floodplain for each SWAT+ channel object, as simulated by the model; (b) locations of wetlands, as delineated by the National Wetlands Inventory of the U.S. Fish and Wildlife Service (accessed November 2023); (c) fraction of time during 2000–2015 that each *gwflow* cell is in connection with the floodplain; and (d) the frequency distribution of inundation for *gwflow* cells experiencing inundation during the simulation period.

captures the general temporal streamflow patterns at both the upstream and downstream gage. According to performance threshold values for monthly streamflow suggested by Moriasi et al. (2015), highlighted values in Table 4 are green for a "good" model fit ($0.7 < NSE \leq 0.8$), yellow for a "satisfactory" model fit ($0.50 < NSE \leq 0.70$; $\pm 10 < PBIAS < \pm 15$), and red for a "not satisfactory" model fit ($PBIAS \geq \pm 15$). Moriasi et al. (2015) do not include KGE in their recommendations and thus those values are not highlighted, but KGE values range from $-\infty$ to 1 with values approaching 1 indicating a better model fit. Visual assessment and model performance metrics indicate that simulated streamflow at the downstream gage site yielded a better fit ($NSE = 0.74$ and 0.71 for the testing period for the floodplain and control scenarios, respectively) than the upstream gage site ($NSE = 0.56$ and 0.57 for the testing period). KGE values were essentially equivalent between the two gage sites for the testing period, with the floodplain scenario showing better performance overall. PBIAS is greater than 15% for each period except for the calibration period of the floodplain scenario, for the downstream gage, indicating that the model is underestimating streamflow, particularly for peak flows (see Figure 7). Likely this is due to difficulties in characterising snowmelt at high elevations, across all catchments of the model.

Simulated groundwater head was between 1.6 m and 23.7 m of observed values, with high residuals occurring due to steep elevation changes in the more mountainous areas where several of the monitoring wells are located (see Figure 4a). The MAPE for the well sites ranged from 0.12% to 0.64%, with small differences between the control and floodplain scenarios. The control scenario slightly outperforms the floodplain scenario, although no wells are located in delineated floodplain areas (compare well locations in Figure 4a to floodplain locations in Figure 4b). In general, there are not enough groundwater observation locations in this mountainous watershed to provide a strong test of groundwater levels near channels. This is true of most high-elevation watersheds, where bead and string analysis is performed. In general, however, spatial groundwater head patterns (Figure 8a) follow the topography of the watershed, with lowest values near the channels. In areas of floodplain exchange, groundwater heads are higher in the floodplain scenario than in the control scenario (Figure 8b), as channels provide recharge to the water table.

3.1.3 | Hydrologic fluxes

While both scenarios yield similar magnitudes of streamflow compared to measured values (Figure 7), the processes of streamflow generation are different between the control and floodplain scenarios. Table 5 provides the average annual flux (in millimetre per year) of each major hydrologic process in the watershed during the 2000–

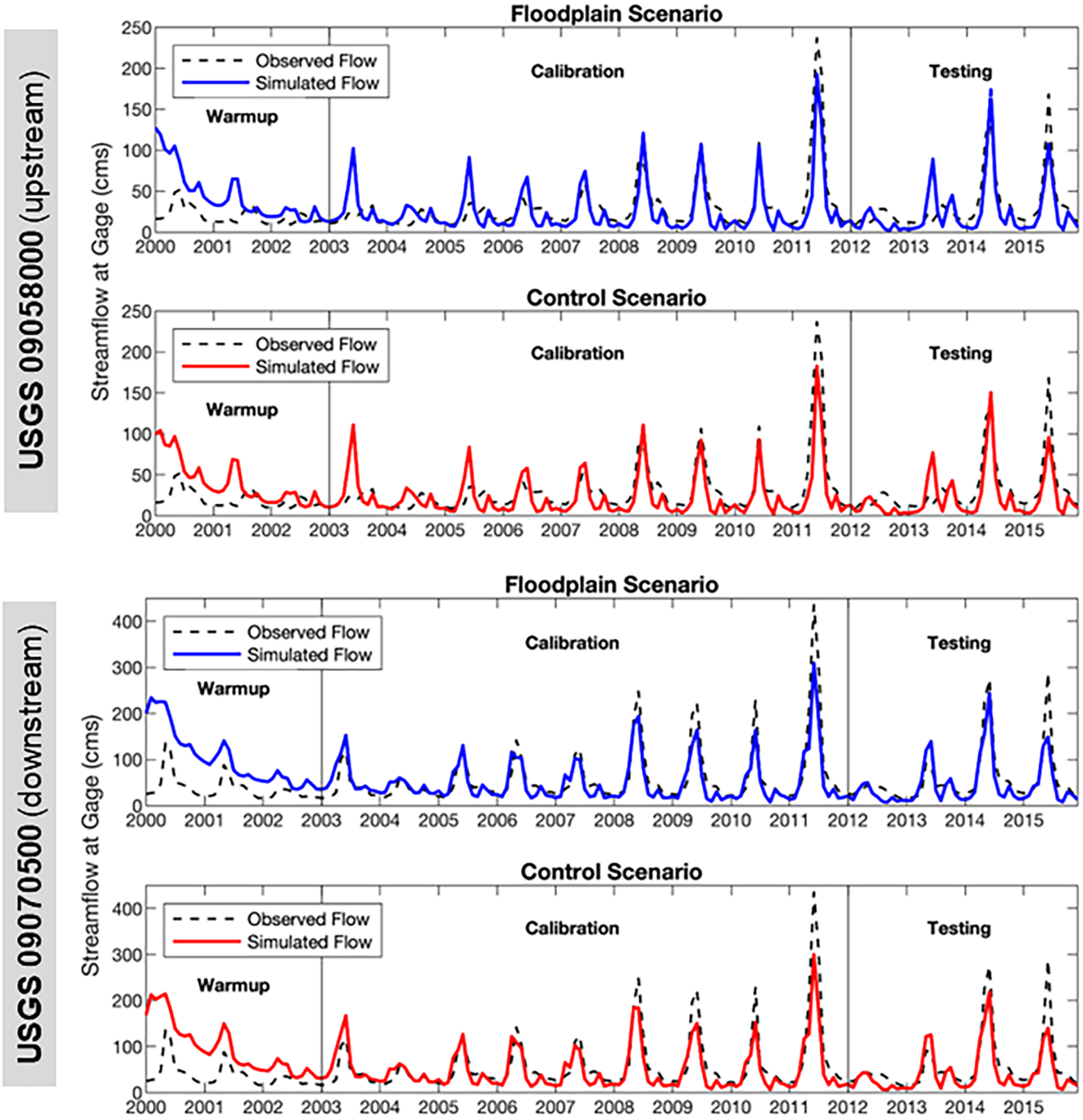

FIGURE 7 Monthly streamflow at the upstream and downstream USGS gage sites.

2015 period. Whereas water yield (surface runoff + soil lateral flow + groundwater saturation excess runoff − channel seepage) is approximately the same between the control (276.8 mm/year) and floodplain (278.6 mm/year) scenarios, the values of each these streamflow generation processes are quite different. The control scenario has much higher surface runoff and soil lateral flow (49.2 and 66.1 mm/year) compared to the floodplain scenario (27.3 and 56.6 mm/year), whereas the floodplain scenario has higher groundwater saturation excess runoff (213 mm/year compared to 166.3 mm/year). Of the three main mechanisms that contribute to streamflow generation, the control scenario has 41% contributed by runoff and soil lateral flow, but only 28% in the floodplain scenario (Figure 9a). These differences are also seen on the annual time scale (Figure 9b).

These differences are due to the processes and parameters available to the PEST calibration software. For the control scenario, attempting to match the required monthly streamflow at the upstream and downstream gage sites yielded high surface runoff (49.2 mm/year) and soil lateral flow (27.3 mm/year). However, within

TABLE 4 Model performance metrics for the upstream and downstream USGS streamflow gage, using monthly streamflow from the SWAT+ model for both the control and floodplain scenarios.

		NSE		PBIAS		KGE		RMSE	
	Period	Floodplain	Control	Floodplain (%)	Control (%)	Floodplain	Control	Floodplain (m^3/s)	Control (m^3/s)
Upstream (09058000)	Calibration	0.64	0.60	15	21	0.74	0.68	20.07	21.19
	Testing	0.56	0.57	23	30	0.70	0.63	21.36	21.14
Downstream (09070500)	Calibration	0.79	0.76	13	16	0.71	0.69	29.38	31.72
	Testing	0.74	0.71	22	27	0.70	0.63	30.27	32.14

Abbreviations: KGE, Kling–Gupta efficiency; NSE, Nash–Sutcliffe model efficiency coefficient; PBIAS, percent bias; RMSE, root-mean-square error.

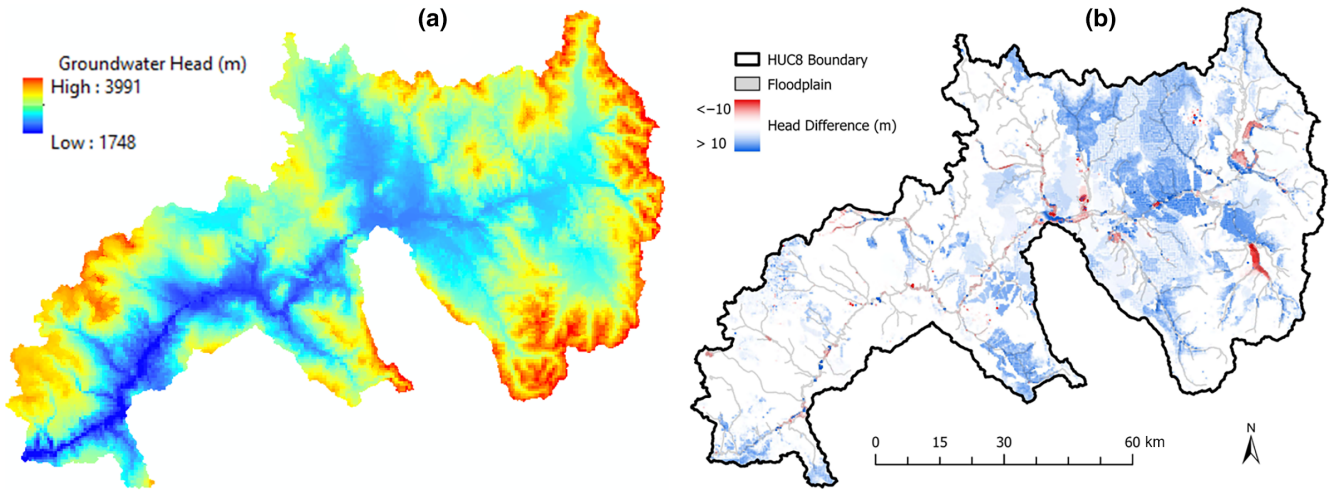

FIGURE 8 (a) Average simulated groundwater head (m) for each grid cell during 2015, for the control scenario; (b) difference (control − floodplain) for the floodplain scenario.

the floodplain scenario, recharge to the aquifer in the floodplain areas (15.7 mm/year) raises the water table, which is already close to the land surface near channels, and in many areas, this rise intersects the ground surface, leading to groundwater saturation excess runoff to channels once the channel flooding has receded. As a result, groundwater saturation excess runoff is much higher in the floodplain scenario, leading to an acceptable simulated streamflow compared to measured values. Thus, even though channel water is lost to the aquifer via floodplain recharge, this additional water in the aquifer eventually returns to the channels. And, because not as much surface runoff and soil lateral flow are required to achieve the correct magnitude of streamflow, more snowmelt and rainfall in the watershed is allowed to infiltrate and percolate, leading to more recharge (see Table 5: 120 mm compared to 89.5 mm, a difference of 34%).

Examining hydrologic fluxes in the floodplain scenario on a daily scale (Figure 10), snowmelt and rainfall in the spring months (April–June; Figure 10a) leads to recharge from the soil profile and recharge from floodplain areas (Figure 10b), which in turn leads to high water tables and groundwater saturation excess flow (Figure 10b) during the same months. The majority of rainfall occurs during summer and fall months (Figure 10a) but, due to high soil ET, extensive recharge to the water table does not occur. For exceptionally wet periods, such as fall 2013 and fall 2014, enough rainfall occurs to produce late-season recharge events (Figure 10b). Recharge during 2012 is minimal due to the relatively low amount of snowmelt compared to other years.

Although the net watershed floodplain-groundwater exchange is floodplain recharge to the aquifer (16 mm/year), groundwater discharge to channels in the floodplain does occur, as evidenced by small negative values (i.e., groundwater leaving the aquifer) in the daily time series of Figure 10b. Annual average floodplain recharge is 18 mm/year, whereas groundwater discharge to channels is 2 mm/year. For approximately two-thirds of the days during 2000–2015, net exchange is floodplain recharge. Net floodplain exchange ranges from 3 mm of recharge during 2012 (see Figure 9b) to 20 mm of recharge during 2003. Note that while the model calculates a volumetric flux over a floodplain cell (i.e., m^3/year), we have divided these fluxes by the floodplain area intersecting each cell to get mm/year, which can be directly compared with other hydrologic fluxes. Figure 11 shows cells where floodplain recharge (red, positive values) and groundwater discharge (blue, negative values) occur.

3.2 | Categorization of floodplain exchange

The number of bead and string cells by threshold value and stream order is summarized in Table 6. Higher threshold values had a

lower percentage of bead cells for each stream order. Using this categorisation, we created datasets of average annual flux values through bead or string cells. If a floodplain cell had no simulated fluxes over the entire 2003–2015 period, we removed it from the dataset.

TABLE 5 Average annual hydrologic fluxes (mm/year) for the control and floodplain scenarios.

Process	Control (mm/year)	Floodplain (mm/year)
Precipitation	589	589
Snowmelt	391	391
Rainfall	198	198
Boundary inflow	34.6	37.6
Soil ET	376	378
Surface runoff	*49.2*	*27.3*
Soil lateral flow	*66.1*	*56.6*
Recharge	89.5	120
Groundwater ET	0.0	0.0
Channel seepage	*4.8*	*2.6*
Saturation excess	*166*	*213*
Irrigation pumping	0.9	1.3
Lake recharge	0.0	0.0
Floodplain exchange	0.0	15.7
Water yield	276.8	278.6

Note: Italicised values indicate processes that either contribute (surface runoff, soil lateral flow, saturation excess flow) or remove (channel seepage) water from the channel system. Water yield = surface runoff + soil lateral flow + saturation excess runoff − channel seepage. The first four hydrologic processes represent overall inputs to the watershed where precipitation = snowfall (snowmelt) + rainfall and boundary inflow is the result of groundwater entering the watershed from the constant head groundwater cells defined at the watershed boundary.

A Kolmogorov–Smirnov test of normality on each dataset (8 total) indicated that none were normally distributed (p-values <<0.001). A non-parametric Mann–Whitney U-test comparing bead and string datasets resulted in p-values of 0.8924, 0.0067, 0.3060, and 0.0406 for thresholds of 3-, 5-, 7-, and 9-times median stream width, respectively. Thus, for a 5% significance level ($\alpha = 0.05$), the null hypothesis that the two datasets are derived from the same population is rejected for thresholds of 5- and 9-times median stream width (i.e., the populations are different), while the 3- and 7-times median stream width datasets fail to reject the null hypothesis (i.e., the data do not show the populations are different). Table 7 lists dataset statistics separated by beads and strings for each cell size.

The boxplots in Figure 12 provide a visual representation of the bead and string datasets for the 5- and 7-times median stream width thresholds. The 5-times threshold had the largest difference in mean values (3.91 mm) while the 7-times threshold had the smallest difference (2.99 mm). Due to many outliers at all cell resolutions, we limited the extent of the boxplots and listed the percent of each dataset classified as outliers on each plot. The minimum and maximum values for each threshold are included in Table 7. Median values for beads and strings at each cell size were equal at 0 mm/day while the mean values had larger differences. The difference between mean bead and mean string flux values was 3.90 mm for the 3-times threshold and 3.28 mm for the 9-times threshold.

We calculated net water volume exchanged for bead and string cells from average annual flux values. For each cell, we multiplied the volumetric flux (m^3/day) by the number of days in each year to calculate a total volume exchanged per year per grid cell. Total volume

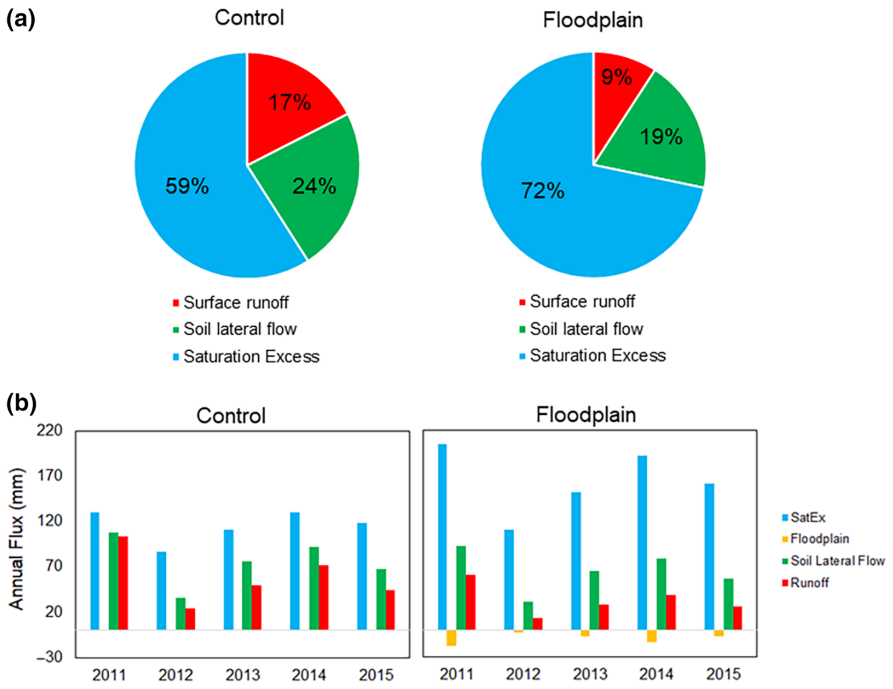

FIGURE 9 (a) Percentage of streamflow generation attributed to surface runoff, soil lateral flow, and groundwater saturation excess flow, for the control and floodplain scenarios; (b) annual fluxes (mm/year) for 2011–2015, for groundwater saturation excess flow, floodplain recharge (seepage from channel), soil lateral flow, and surface runoff.

exchanged by bead and string cells per year was the sum of these volumes by category. Figure 13 shows plots of these values for the 5- and 7-times threshold widths. In addition, we summed total exchange volumes over the period 2003–2015 for bead and string cells. To account for higher bead areas compared to string areas, we normalized the data by dividing total exchange volume by the area of each floodplain category. Table 8 summarizes total volumes, normalized volumes, and area by threshold value and bead or string. We calculated the percent difference between bead and string volumes and areas using Equation (11).

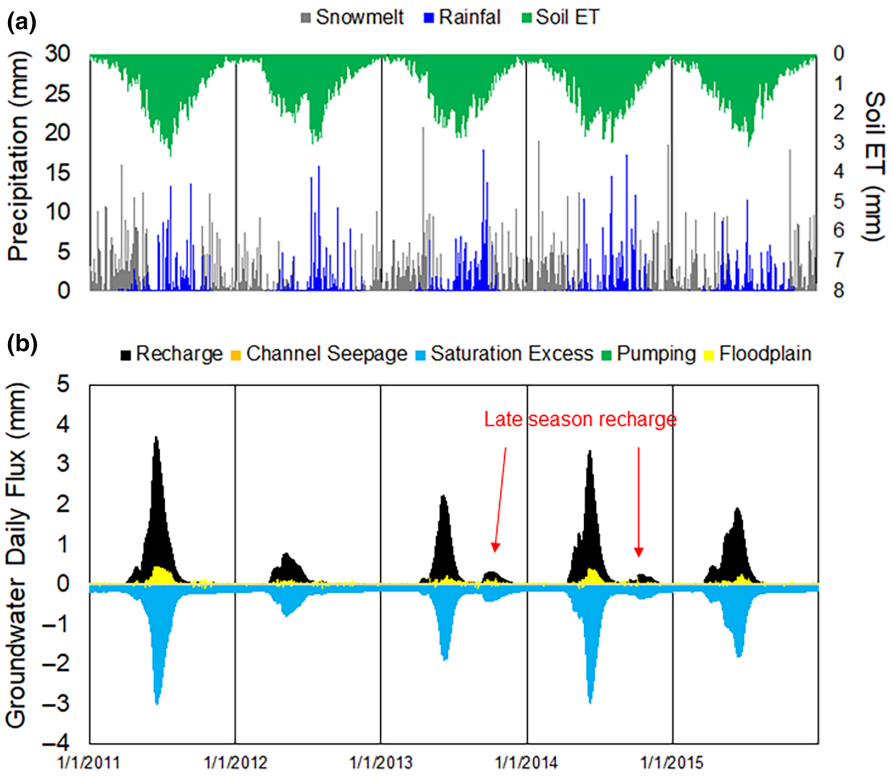

FIGURE 10 Daily fluxes of (a) snowmelt, rainfall, and soil ET; (b) recharge, saturation excess runoff, pumping, floodplain exchange, and channel seepage. Pumping and channel seepage are small in comparison to the other fluxes.

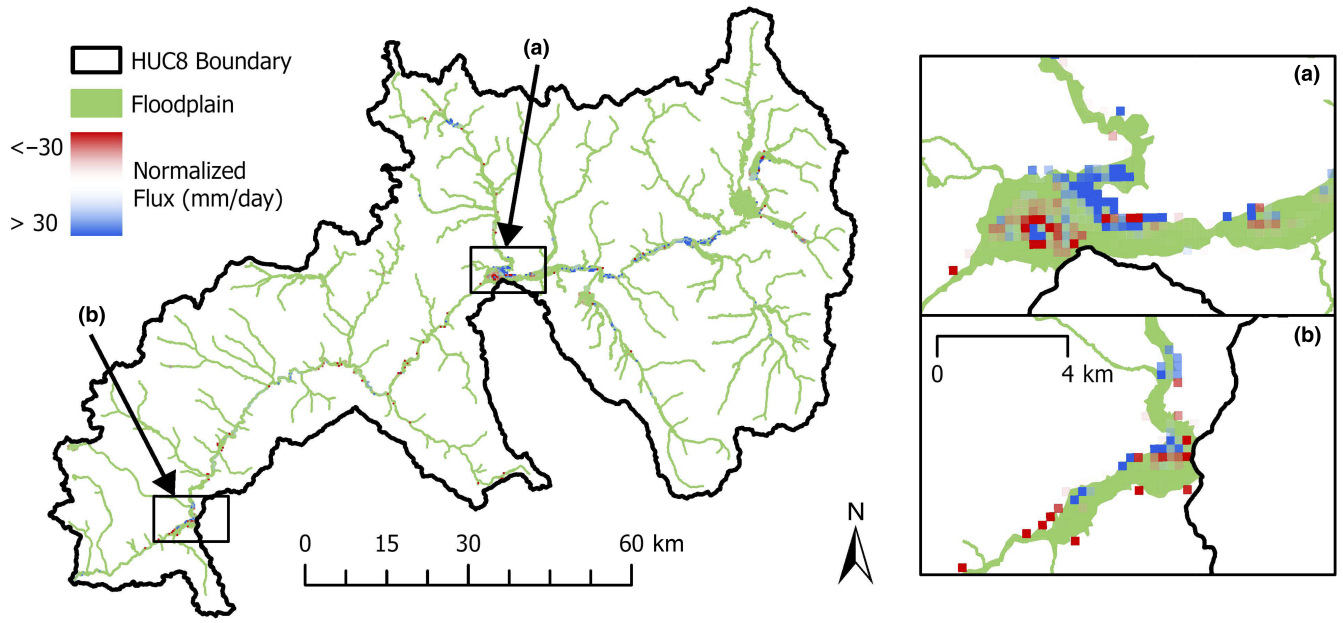

FIGURE 11 Annual floodplain fluxes simulated in the year 2014, showing local areas of high floodplain exchange activity in (a) and (b). Floodplain regions that do not show exchange rates may not have experienced overbank flows or may have had a minimal hydraulic gradient that did not facilitate infiltration/exfiltration from groundwater (i.e., the head differential and/or hydraulic conductivity were too small).

TABLE 6 Quantification of the number of bead and string cells in the study watershed by stream order.

Threshold	Stream order	Floodplain cells	Bead cells	String cells	% bead
3×	4	1993	1867	126	93.7
	5	568	528	40	93.0
	6	1716	912	804	53.1
5×	4	1993	1690	303	84.8
	5	568	477	91	84.0
	6	1716	679	1037	39.6
7×	4	1993	1551	442	77.8
	5	568	399	169	70.2
	6	1716	549	1167	32.0
9×	4	1993	1460	533	73.3
	5	568	318	250	56.0
	6	1716	424	1292	24.7

TABLE 7 Statistics for bead and string flux datasets from 2003 to 2015.

Threshold	Statistic (mm/day)	Bead	String
3×	Mean	3.582	−0.320
	Median	0.000	0.000
	Maximum	387.200	93.921
	Minimum	−288.878	−93.862
5×	Mean	3.954	0.044
	Median	0.000	0.000
	Maximum	387.200	101.409
	Minimum	−288.878	−121.906
7×	Mean	3.897	0.910
	Median	0.000	0.000
	Maximum	387.200	379.979
	Minimum	−288.878	−121.906
9×	Mean	4.225	0.943
	Median	0.000	0.000
	Maximum	387.200	379.979
	Minimum	−288.878	−121.906

$$\%\text{Difference} = \left(\frac{\text{bead} - \text{string}}{\text{string}}\right) 100. \quad (11)$$

Bead cells simulated a substantially higher total exchange volume compared to string cells for all threshold widths, with exchange volumes 863% higher on average. Normalisation of exchange volume by area reduced the percent differences, but still indicated higher exchange through bead cells (average 146% higher). Total volume exchanged through bead cells was also higher in each individual year than for string cells (Figure 13). Total simulated exchange volume through bead regions increased with reduced threshold width, likely due to the higher percentage of bead cells relative to string cells calculated for lower thresholds (Table 8).

4 | DISCUSSION

4.1 | Inclusion of floodplain-groundwater interactions

When compared to measured streamflow, the model including floodplain-groundwater exchange performed as well or better than the control model. Although the control model without floodplain interactions performed well, it was not fully accounting for floodplain-groundwater exchanges, which required it to overestimate surface runoff and lateral flow. With the addition of floodplain-groundwater exchange through the *gwflow* module, it is reasonable to assume that the representation of processes is better in the updated model compared to the control model (even with large curve number values). The floodplain scenario also provided valuable information about floodplain inundation and exchange rates in the study watershed. From these results, we conclude that the addition of floodplain-groundwater exchange in the *gwflow* module of SWAT+ improves the model's representation of hydrological processes in watersheds since it has similar performance while including another realistic hydrologic exchange pathway.

The volume of water exchanged between channels in floodplains and groundwater was non-negligible, contributing 6% of simulated channel-related exchanges. Understanding how these individual hydrologic exchanges contribute to streamflow is essential for accurately simulating watershed hydrology. Floodplains are an additional source of groundwater recharge. Quantification of these processes in the field or further studies are necessary to fully validate these results; however, considering model performance metrics and the physically based approach of the *gwflow* module, these floodplain processes are a substantial hydrologic exchange pathway in the study watershed. In addition, the incorporation of floodplain exchange in SWAT+ results in a more physically based, realistic representation of hydrologic processes. The current algorithms in SWAT+ only simulate flow from a floodplain to an aquifer and do not account for groundwater depth.

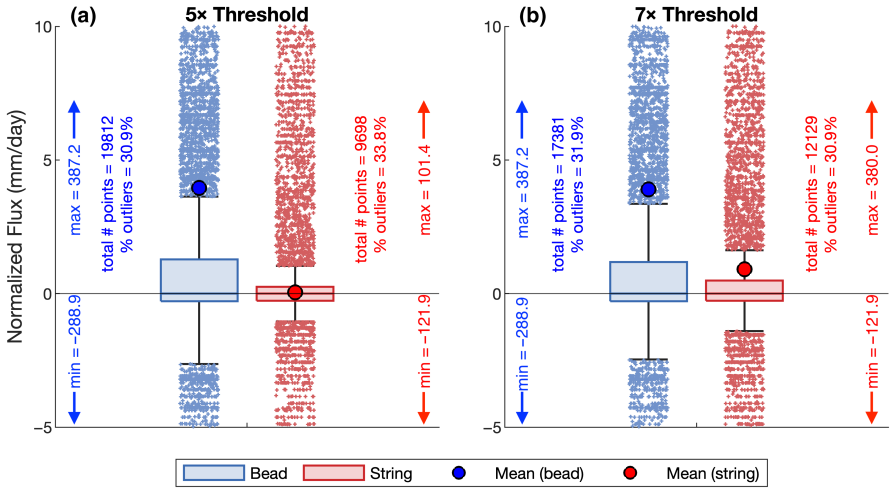

FIGURE 12 Normalized average annual floodplain flux by bead and string cells simulated from 2003 to 2015.

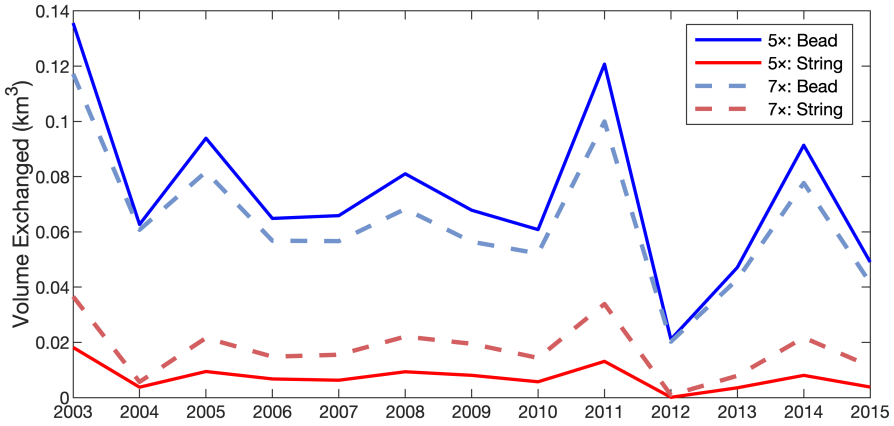

FIGURE 13 Total simulated recharge, discharge, and net volume exchanged by bead and string cells from 2003 to 2015 for 5- and 7-times median stream width threshold values.

TABLE 8 Total and normalized exchange volumes summed over 2003–2015 by beads and strings.

	Threshold	Bead	String	% difference
Total volume (km^3)	3×	1.012	0.046	2108.6
	5×	0.962	0.096	899.9
	7×	0.832	0.226	268.4
	9×	0.776	0.282	175.3
Normalized volume (m)	3×	9.358	2.461	280.2
	5×	9.788	3.373	190.2
	7×	9.289	6.072	53.0
	9×	9.662	6.068	59.2
Area (km^2)	3×	108.18	18.63	480.8
	5×	98.29	28.53	244.6
	7×	89.60	37.21	140.8
	9×	80.34	46.47	72.9

An accurate understanding of watershed processes is particularly valuable for this study watershed, which is part of the larger Colorado River basin, one of the most regulated hydrologic systems in the world (Graf, 1985). Impacts to this headwater system can have cascading effects downstream, so thoughtful management and protection of water resources in this system could potentially benefit countless water users. This is especially important as the river network faces climate-related challenges (Bair et al., 2019) that could include increasing human consumption, diminishing flows (Christensen et al., 2004), and declining riparian ecosystem health (Sankey et al., 2015).

4.2 | Quantification and categorization of floodplain fluxes

Many studies have assessed the function of floodplain beads compared to strings. Beads in old-growth forests have higher wood loads than in strings (Livers & Wohl, 2016; Polvi & Wohl, 2013), which in turn leads to higher spatial heterogeneity (Wohl et al., 2017). Spatial heterogeneity improves the availability and diversity of habitat (Wohl et al., 2017), benefits biological productivity and species richness (Bellmore & Baxter, 2014; Hauer et al., 2016; Hood & Larson, 2014), and increases organic carbon retention (Wohl et al., 2012). These studies emphasise the importance of bead regions, although they focus on surface processes which are often easier to assess visually or through field studies. Groundwater processes, especially flux rates, are much more difficult to assess as they are not as easily measured or visualized. Moreover, quantifying processes at a watershed scale is often infeasible due to access constraints and the amount of data required.

This study introduces a novel approach for quantifying channel-groundwater interactions through bead and string regions of a river corridor. Our analyses on the location of floodplain fluxes within the watershed showed that beads had a higher net and per area volume of floodplain-groundwater exchange than strings. These outputs are consistent across all threshold bead widths, with lower threshold widths simulating greater differences between bead and string floodplain regions. We also found that flux rates through bead regions were higher than for string regions, and these results are statistically significant for 5- and 9-times median stream width. While this quantification focuses on floodplain-groundwater exchange, which is only one exchange pathway present in the complex mosaic of floodplain processes, it confirms existing field studies and our conceptual understanding of how beads function.

Land use changes and reductions in forest cover often impact bead function (Wohl & Beckman, 2014) despite how important floodplain beads are for protecting river system resilience and ecosystem function (Hauer et al., 2016; Wohl et al., 2017). Future land management and conservation practises should prioritize these key locations that improve ecosystem health. In addition, process-based restoration techniques, which often emphasise reconnecting channels and floodplains (Ciotti et al., 2021), may see additional benefits to floodplain-groundwater processes, especially when restoration efforts target beads within a catchment (Wohl et al., 2024). Results from our study further confirm the importance of floodplain beads, specifically in the context of floodplain-groundwater exchange. Through this modelling effort, we show that floodplain beads have disproportionately higher volumes and flux rates of hydrologic exchange than strings. Thus, in addition to their improved surface heterogeneity, storage, and biological productivity, we conclude that beads are important locations for groundwater interactions.

4.3 | Study limitations

There were several limitations to this study. We only performed calibration for models with a grid cell size of 1000 m, which was the smallest cell size feasible due to time and large computing constraints. Furthermore, we did not calibrate models to groundwater well data due to limited well locations. While there are wells within the watershed that have measured groundwater head during the study period, they were clustered closely together and did not seem representative of groundwater head for the overall watershed. Some analysis was still performed to assess model fit, but none of the models were directly calibrated to well data.

The analysis cell resolution of 250 m is coarse when considering the complexity of floodplain processes. For this study, this cell size was the smallest resolution that provided reasonable model run times. The GFPLAIN resolution also limited analysis, as it was produced at a resolution of 30 m, which was not sufficient for analysis of stream orders 1–3 in the watershed. We encourage future studies to explore methods that consider the importance on smaller stream orders on groundwater exchange, especially since low order streams comprise the largest cumulative stream lengths (Downing et al., 2012).

Dams can impact surface water-groundwater interactions, both in the vicinity of a reservoir (Jiang et al., 2024) and downstream of the dam due to fluctuating flow releases (e.g., Ferencz et al., 2019). Our study did not specifically identify dam locations and assess the hydrologic implications of dams in the Colorado headwaters, though we anticipate that any local additional aquifer recharge in the vicinity of reservoirs would be more than offset by loss of floodplain connectivity downstream of dams due to flow regulation (e.g., Ward & Stanford, 1995). Loss of floodplain connectivity would likely reduce floodplain-groundwater exchange, especially in beads.

Finally, we applied models to a montane region in the western United States, which is not representative of the many variations in climate, land use, soil, and aquifer properties that exist worldwide. In addition, as with many montane regions, our study site included limited historical groundwater data that we could use for calibration and validation of our SWAT+ model. The lack of groundwater data makes it difficult to assess the accuracy of the conductivity and specific yield parameter values used in our model. However, since we did not change the values between modelled scenarios, we do not expect the general results of our study to be impacted.

The results presented here should not be extrapolated to other regions without further study. The analysis on bead and string locations is also limited by this study location, and the patterns noted here require additional verification at other study sites.

5 | CONCLUSIONS

In this study, we found that SWAT+ models that use the *gwflow* model for the Colorado headwaters watershed can reasonably simulate observed streamflow at two USGS gage locations. Models that include floodplain exchanges with the aquifer in *gwflow* meet or exceed model performance metrics compared to the control (no floodplain exchange) scenario and improve the representation of hydrologic pathways in the model. Recharge of channel water to the aquifer in floodplain areas raises the water table to the ground surface, leading to groundwater saturation excess runoff and discharge

back to channels. Due to the inclusion of this process, surface runoff and soil lateral flow fluxes were lower than in the control scenario, as the increased groundwater discharge can meet the measured streamflow rates.

Analyses of floodplain fluxes indicate that bead regions of the floodplain exchange a higher volume of water, both net and by area, than string regions. Mean values of normalized flux are also higher in bead regions than in string regions. Thus, model results suggest that efforts to conserve or protect floodplain channel-groundwater exchanges in this watershed should focus on wider floodplain regions (beads) to preserve a larger proportion of hydrologic interactions.

While lower order streams encompass the majority proportion of stream length globally (Downing et al., 2012) and thus have equivalently abundant riparian corridors, our floodplain delineation procedure did not have a fine enough resolution for accurate assessment. Studying floodplain channel-groundwater exchanges in these smaller streams should be a priority for future work to understand their impacts on watershed processes. For an analysis of lower stream orders, a finer resolution floodplain delineation procedure could provide enough detail to analyse changes in floodplain width and thus improve bead and string categorization at that scale. However, these analyses would likely require proprietary datasets and a smaller model scope to allow for reasonable run times. Analyses of lower order streams should be coupled with an equivalent reduction in *gwflow* grid cell size, to replicate the spatial extent of floodplains more accurately.

To verify performance for various conditions, further studies should apply the updated SWAT+ model with floodplain exchange to watersheds with different climate, surface/subsurface properties, and sizes. Model testing should be performed at locations of groundwater wells where groundwater level data are available. To better capture spatial variations, additional aquifer and floodplain soil property zones could be included in future *gwflow* module setups, and a more detailed SWAT+ modelling framework could be created. Finally, ground truthing of simulated exchange processes would provide valuable insight into model accuracy.

ACKNOWLEDGEMENTS

This work was supported by the USDA National Institute of Food and Agriculture, Hatch project COL00425, accession number 7002851. Support was also provided by NSF awards 2115169 and 2142761 and a grant from the Walton Family Foundation. We thank Ellen Wohl for her initial review of this work.

DATA AVAILABILITY STATEMENT

The data associated with the results of this study can be found at: http://www.hydroshare.org/resource/3ba513e0a47849a398ec8dba9e8df49a.

ORCID

Ryan R. Morrison https://orcid.org/0000-0002-8612-1684

REFERENCES

Andersen, D. C., Cooper, D. J., & Northcott, K. (2007). Dams, floodplain land use, and riparian forest conservation in the semiarid upper Colorado River basin, USA. *Environmental Management*, *40*(3), 453–475. https://doi.org/10.1007/s00267-006-0294-7

Andersen, H. E. (2004). Hydrology and nitrogen balance of a seasonally inundated Danish floodplain wetland. *Hydrological Processes*, *18*(3), 415–434. https://doi.org/10.1002/hyp.1277

Annis, A., Nardi, F., Morrison, R. R., & Castelli, F. (2019). Investigating hydrogeomorphic floodplain mapping performance with varying DTM resolution and stream order. *Hydrological Sciences Journal*, 1–14. https://doi.org/10.1080/02626667.2019.1591623

Arnold, J. G., Srinivasan, R., Muttiah, R. S., & Williams, J. R. (1998). Large area hydrologic modeling and assessment part I: Model development1. *JAWRA Journal of the American Water Resources Association*, *34*(1), 73–89. https://doi.org/10.1111/j.1752-1688.1998.tb05961.x

Arnold, J. G., White, M. J., Allen, P. M., Gassman, P. W., & Bieger, K. (2021). Conceptual framework of connectivity for a national agroecosystem model based on transport processes and management practices. *JAWRA Journal of the American Water Resources Association*, *57*(1), 154–169. https://doi.org/10.1111/1752-1688.12890

Bailey, R. T., Abbas, S., Arnold, J., White, M., Gao, J., & Čerkasova, N. (2023). Augmenting the national agroecosystem model with physically based spatially distributed groundwater modeling. *Environmental Modelling & Software*, *160*, 105589. https://doi.org/10.1016/j.envsoft.2022.105589

Bailey, R. T., Bieger, K., Arnold, J. G., & Bosch, D. D. (2020). A new physically-based spatially-distributed groundwater flow module for SWAT+. *Hydrology*, *7*(4), 75. https://doi.org/10.3390/hydrology7040075

Bailey, R. T., Bieger, K., Flores, L., & Tomer, M. (2022). Evaluating the contribution of subsurface drainage to watershed water yield using SWAT + with groundwater modeling. *Science of the Total Environment*, *802*, 149962. https://doi.org/10.1016/j.scitotenv.2021.149962

Bailey, R., & Alderfer, C. (2022). Groundwater data in unconfined aquifers—Conterminous United States. *Figshare*. https://doi.org/10.6084/m9.figshare.c.5918738.v2

Bair, L. S., Yackulic, C. B., Schmidt, J. C., Perry, D. M., Kirchhoff, C. J., Chief, K., & Colombi, B. J. (2019). Incorporating social-ecological considerations into basin-wide responses to climate change in the Colorado River basin. *Current Opinion in Environmental Sustainability*, *37*, 14–19. https://doi.org/10.1016/j.cosust.2019.04.002

Bates, P. D., Stewart, M. D., Desitter, A., Anderson, M. G., Renaud, J. P., & Smith, J. A. (2000). Numerical simulation of floodplain hydrology. *Water Resources Research*, *36*(9), 2517–2529. https://doi.org/10.1029/2000WR900102

Bellmore, J. R., & Baxter, C. V. (2014). Effects of geomorphic process domains on river ecosystems: A comparison of floodplain and confined valley segments. *River Research and Applications*, *30*(5), 617–630. https://doi.org/10.1002/rra.2672

Bieger, K., Arnold, J. G., Rathjens, H., White, M. J., Bosch, D. D., & Allen, P. M. (2019). Representing the connectivity of upland areas to floodplains and streams in SWAT+. *JAWRA Journal of the American Water Resources Association*, *55*(3), 578–590. https://doi.org/10.1111/1752-1688.12728

Bieger, K., Arnold, J. G., Rathjens, H., White, M. J., Bosch, D. D., Allen, P. M., Volk, M., & Srinivasan, R. (2017). Introduction to SWAT+, a completely restructured version of the soil and water assessment tool. *JAWRA Journal of the American Water Resources Association*, *53*(1), 115–130. https://doi.org/10.1111/1752-1688.12482

Boulton, A. J., Findlay, S., Marmonier, P., Stanley, E. H., & Valett, H. M. (1998). The functional significance of the hyporheic zone in streams and rivers. *Annual Review of Ecology and Systematics*, *29*, 59–81.

Brunke, M., & Gonser, T. (1997). The ecological significance of exchange processes between rivers and groundwater. *Freshwater Biology*, *37*(1), 1–33. https://doi.org/10.1046/j.1365-2427.1997.00143.x

Brunner, P., Simmons, C. T., & Cook, P. G. (2009). Spatial and temporal aspects of the transition from connection to disconnection between

rivers, lakes and groundwater. *Journal of Hydrology*, *376*(1), 159–169. https://doi.org/10.1016/j.jhydrol.2009.07.023

Caldwell, P. V., Sun, G., McNulty, S. G., Cohen, E. C., & Moore Myers, J. A. (2012). Impacts of impervious cover, water withdrawals, and climate change on river flows in the conterminous US. *Hydrology and Earth System Sciences*, *16*(8), 2839–2857. https://doi.org/10.5194/hess-16-2839-2012

Cartwright, I., Werner, A. D., & Woods, J. A. (2019). Using geochemistry to discern the patterns and timescales of groundwater recharge and mixing on floodplains in semi-arid regions. *Journal of Hydrology*, *570*, 612–622. https://doi.org/10.1016/j.jhydrol.2019.01.023

Christensen, N. S., Wood, A. W., Voisin, N., Lettenmaier, D. P., & Palmer, R. N. (2004). The effects of climate change on the hydrology and water resources of the Colorado River basin. *Climatic Change*, *62*(1), 337–363. https://doi.org/10.1023/B:CLIM.0000013684.13621.1f

Ciotti, D. C., Mckee, J., Pope, K. L., Kondolf, G. M., & Pollock, M. M. (2021). Design criteria for process-based restoration of fluvial systems. *Bioscience*, *71*, 831–845. https://doi.org/10.1093/biosci/biab065

Costanza, R., d'Arge, R., de Groot, R., Farber, S., Grasso, M., Hannon, B., Limburg, K., Naeem, S., O'Neill, R. V., Paruelo, J., Raskin, R. G., Sutton, P., & van den Belt, M. (1997). The value of the world's ecosystem services and natural capital. *Nature*, *387*, 253–260. https://doi.org/10.1038/387253a0

de Vente, J., Poesen, J., Verstraeten, G., Govers, G., Vanmaercke, M., Van Rompaey, A., Arabkhedri, M., & Boix-Fayos, C. (2013). Predicting soil erosion and sediment yield at regional scales: Where do we stand? *Earth-Science Reviews*, *127*, 16–29. https://doi.org/10.1016/j.earscirev.2013.08.014

Dewitz, J. (2023). National Land Cover Database (NLCD) 2021 Products: U.S. Geological Survey data release. https://www.sciencebase.gov/catalog/item/647626cbd34e4e58932d9d4e

Dieter, C. A., Maupin, M. A., Caldwell, R. R., Harris, M. A., Ivahnenko, T. I., Lovelace, J. K., Barber, N. L., & Linsey, K. S. (2018). *Estimated use of water in the United States in 2015: U.S. Geological Survey Circular 1441* (p. 76). U.S. Geological Survey.

Doherty, J. (2018). *PEST user manual* (7th ed.). Watermark Numerical Computing.

Downing, J. A., Cole, J. J., Duarte, C. M., Middelburg, J. J., Melack, J. M., Prairie, Y. T., Kortelainen, P., Striegl, R. G., McDowell, W. H., & Tranvik, L. J. (2012). Global abundance and size distribution of streams and rivers. *Inland Waters*, *2*(4), 229–236. https://doi.org/10.5268/IW-2.4.502

Fan, Y., Li, H., & Miguez-Macho, G. (2013). Global patterns of groundwater table depth. *Science*, *339*(6122), 940–943. https://doi.org/10.1126/science.1229881

Ferencz, S. B., Cardenas, M. B., & Neilson, B. T. (2019). Analysis of the effects of dam release properties and ambient groundwater flow on surface water-groundwater exchange over a 100-km-long reach. *Water Resources Research*, *55*, 8526–8546. https://doi.org/10.1029/2019WR025210

Gesch, D. B., Evans, G. A., Oimoen, M. J., & Arundel, S. (2018). *The National Elevation Dataset*. U.S. Geological Survey.

Goodrich, D. C., Williams, D. G., Unkrich, C. L., Hogan, J. F., Scott, R. L., & Hultine, K. R. (2004). Comparison of methods to estimate ephemeral channel recharge, walnut gulch, San Pedro River basin, Arizona. In *Groundwater recharge in a desert environment: The southwestern United States* (pp. 77–99). American Geophysical Union.

Graf, W. L. (1985). *The Colorado River: Instability and basin management*. Association of American Geographers.

Hauer, R. F., Locke, H., Dreitz, V. J., Hebblewhite, M., Lowe, W. H., Muhlfeld, C. C., Nelson, C. R., Proctor, M. F., & Rood, S. B. (2016). Gravel-bed river floodplains are the ecological nexus of glaciated mountain landscapes. *Science Advances*, *2*, e1600026. https://doi.org/10.1126/sciadv.1600026

Helton, A. M., Poole, G. C., Payn, R. A., Izurieta, C., & Stanford, J. A. (2014). Relative influences of the river channel, floodplain surface, and alluvial aquifer on simulated hydrologic residence time in a montane river floodplain. *Geomorphology*, *205*, 17–26. https://doi.org/10.1016/j.geomorph.2012.01.004

Hood, G. A., & Larson, D. G. (2014). Beaver-created habitat heterogeneity influences aquatic invertebrate assemblages in boreal Canada. *Wetlands*, *34*, 19–29. https://doi.org/10.1007/s13157-013-0476-z

Horton, J. D. (2017). *The state geologic map compilation (SGMC) geodatabase of the conterminous United States: U.S. geological survey data release*. U.S. Geological Survey.

Jiang, W., Liu, B., Li, Y., Lu, C., & Shu, L. (2024). The effects of damming and dam regulation on a river–lake-aquifer system: 3D groundwater flow modeling of Poyang lake (China). *Journal of Hydrology*, *636*, 131311. https://doi.org/10.1016/j.jhydrol.2024.131311

Junk, W. J., Bayley, P. B., & Sparks, R. E. (1989). The flood pulse concept in river-floodplain systems. *Canadian Special Publications Fisheries and Aquatic Sciences*, *106*, 110–127.

Knox, R. L., Morrison, R. R., & Wohl, E. E. (2022). Identification of artificial levees in the contiguous United States. *Water Resources Research*, *58*(4), e2021WR031308. https://doi.org/10.1029/2021WR031308

Krause, S., Bronstert, A., & Zehe, E. (2007). Groundwater–surface water interactions in a north German lowland floodplain – Implications for the river discharge dynamics and riparian water balance. *Journal of Hydrology*, *347*(3), 404–417. https://doi.org/10.1016/j.jhydrol.2007.09.028

Liechti, T. C., Matos, J. P., Ferràs Segura, D., Boillat, J.-L., & Schleiss, A. J. (2014). Hydrological modelling of the Zambezi River basin taking into account floodplain behaviour by a modified reservoir approach. *International Journal of River Basin Management*, *12*(1), 29–41. https://doi.org/10.1080/15715124.2014.880707

Livers, B., & Wohl, E. (2016). Sources and interpretation of channel complexity in forested subalpine streams of the Southern Rocky Mountains. *Water Resources Research*, *52*, 3910–3929. https://doi.org/10.1002/2015WR018306

Maier, N., Breuer, L., & Kraft, P. (2017). Prediction and uncertainty analysis of a parsimonious floodplain surface water-groundwater interaction model. *Water Resources Research*, *53*(9), 7678–7695. https://doi.org/10.1002/2017WR020749

Martinet, M. C., Vivoni, E. R., Cleverly, J. R., Thibault, J. R., Schuetz, J. F., & Dahm, C. N. (2009). On groundwater fluctuations, evapotranspiration, and understory removal in riparian corridors. *Water Resources Research*, *45*(5), W05425. https://doi.org/10.1029/2008WR007152

Moore, R. B., & Dewald, T. G. (2016). The road to NHDPlus—Advancements in digital stream networks and associated catchments. *JAWRA Journal of the American Water Resources Association*, *52*(4), 890–900.

Moriasi, D. N., Gitau, M. W., Pai, N., & Daggupati, P. (2015). Hydrologic and water quality models: Performance measures and evaluation criteria. *Transactions of the ASABE*, *58*(6), 1763–1785. https://doi.org/10.13031/trans.58.10715

Nanson, G. C., & Croke, J. C. (1992). A genetic classification of floodplains. *Geomorphology*, *4*(6), 459–486. https://doi.org/10.1016/0169-555X(92)90039-Q

Nardi, F., Annis, A., Di Baldassarre, G., Vivoni, E. R., & Grimaldi, S. (2019). GFPLAIN250m, a global high-resolution dataset of Earth's floodplains. *Scientific Data*, *6*(1), 180309. https://doi.org/10.1038/sdata.2018.309

Nardi, F., Morrison, R. R., Annis, A., & Grantham, T. E. (2018). Hydrologic scaling for hydrogeomorphic floodplain mapping: Insights into human-induced floodplain disconnectivity. *River Research and Applications*, *34*(7), 675–685. https://doi.org/10.1002/rra.3296

Neitsch, S. L., Arnold, J. G., Kiniry, J. R., & Williams, J. R. (2009). *Soil and water assessment tool theoretical documentation version 2009*. Texas Water Resources Institute.

Opperman, J. J., Luster, R., McKenney, B. A., Roberts, M., & Meadows, A. W. (2010). Ecologically functional floodplains:

Connectivity, flow regime, and scale. *JAWRA Journal of the American Water Resources Association*, *46*(2), 211–226. https://doi.org/10.1111/j.1752-1688.2010.00426.x

Petsch, H. E., Jr. (1985). *Inventory of inter-basin transfers of water in the western conterminous United States*. U.S. Geological Survey.

Phiri, W. K., Vanzo, D., Banda, K., Nyirenda, E., & Nyambe, I. A. (2021). A pseudo-reservoir concept in SWAT model for the simulation of an alluvial floodplain in a complex tropical river system. *Journal of Hydrology: Regional Studies*, *33*, 100770. https://doi.org/10.1016/j.ejrh.2020.100770

Polvi, L. E., & Wohl, E. (2013). Biotic drivers of stream planform: Implications for understanding the past and restoring the future. *Bioscience*, *63*(6), 439–452. https://doi.org/10.1525/bio.2013.63.6.6

Rajib, A., Liu, Z., Merwade, V., Tavakoly, A. A., & Follum, M. L. (2020). Towards a large-scale locally relevant flood inundation modeling framework using SWAT and LISFLOOD-FP. *Journal of Hydrology*, *581*, 124406. https://doi.org/10.1016/j.jhydrol.2019.124406

Saksena, S., & Merwade, V. (2017). Integrated modeling of surface-subsurface processes to understand river-floodplain hydrodynamics in the upper Wabash River basin. In *World Environmental and Water Resources Congress 2017*, Sacramento, California, May 21–25 (pp. 60–68). The American Society of Civil Engineers. https://doi.org/10.1061/9780784480595.006

Sankey, J. B., Ralston, B. E., Grams, P. E., Schmidt, J. C., & Cagney, L. E. (2015). Riparian vegetation, Colorado River, and climate: Five decades of spatiotemporal dynamics in the grand canyon with river regulation. *Journal of Geophysical Research: Biogeosciences*, *120*(8), 1532–1547. https://doi.org/10.1002/2015JG002991

Shangguan, W., Hengl, T., Mendes de Jesus, J., Yuan, H., & Dai, Y. (2017). Mapping the global depth to bedrock for land surface modeling. *Journal of Advances in Modeling Earth Systems*, *9*(1), 65–88. https://doi.org/10.1002/2016MS000686

Skinner, K. D., & Maupin, M. A. (2019). *Point-source nutrient loads to streams of the conterminous United States, 2012: U.S. Geological Survey Data Series 1101* (p. 24). U.S. Geological Survey. https://doi.org/10.3133/ds1101

Soil Survey Staff. (2011). *Natural Resources Conservation Service, United States Department of Agriculture*. Soil Survey Geographic (SSURGO) Database [Data set]. https://sdmdataaccess.sc.egov.usda.gov

Soil Survey Staff. (2014). *Gridded soil survey geographic (gSSURGO) database for the conterminous United States*. United States Department of Agriculture.

Stanford, J. A., & Ward, J. V. (1993). An ecosystem perspective of alluvial rivers: Connectivity and the hyporheic corridor. *Journal of the North American Benthological Society*, *12*(1), 48–60. https://doi.org/10.2307/1467685

Stanford, J. A., Ward, J. V., Liss, W. J., Frissell, C. A., Williams, R. N., Lichatowich, J. A., & Coutant, C. C. (1996). A general protocol for restoration of regulated rivers. *Regulated Rivers: Research & Management*, *12*(4–5), 391–413. https://doi.org/10.1002/(SICI)1099-1646(199607)12:4/5<391::AID-RRR436>3.0.CO;2-4

Sun, X., Bernard-Jannin, L., Grusson, Y., Sauvage, S., Arnold, J., Srinivasan, R., & Sánchez Pérez, J. M. (2018). Using SWAT-LUD model to estimate the influence of water exchange and shallow aquifer denitrification on water and nitrate flux. *Water*, *10*(4), 528. https://doi.org/10.3390/w10040528

Sun, X., Bernard-Jannin, L., Sauvage, S., Garneau, C., Arnold, J. G., Srinivasan, R., & Sánchez-Pérez, J. M. (2016). Assessment of the denitrification process in alluvial wetlands at floodplain scale using the SWAT model. *Ecological Engineering*, *103*, 344–358. https://doi.org/10.1016/j.ecoleng.2016.06.098

Tockner, K., & Stanford, J. (2002). Review of: Riverine flood plains: Present state and future trends. *Environmental Conservation*, *29*(3), 308–330.

Tonina, D., & Buffington, J. M. (2009). Hyporheic exchange in mountain rivers I: Mechanics and environmental effects. *Geography Compass*, *3*(3), 1063–1086. https://doi.org/10.1111/j.1749-8198.2009.00226.x

U.S. Geological Survey. (2016). National Water Information System data available on the World Wide Web (USGS Water Data for the Nation), http://waterdata.usgs.gov/nwis/

Valayamkunnath, P., Barlage, M., Chen, F., Gochis, D. J., & Franz, K. J. (2020). Mapping of 30-meter resolution tile-drained croplands using a geospatial modeling approach. *Scientific Data*, *7*(1), 1. https://doi.org/10.1038/s41597-020-00596-x

Ward, J. V., & Stanford, J. A. (1995). Ecological connectivity in alluvial river ecosystems and its disruption by flow regulation. *Regulated Rivers: Research & Management*, *11*, 105–119. https://doi.org/10.1002/rrr.3450110109

Ward, J. V., Tockner, K., & Schiemer, F. (1999). Biodiversity of floodplain river ecosystems: Ecotones and connectivity1. *Regulated Rivers: Research & Management*, *15*(1–3), 125–139. https://doi.org/10.1002/(SICI)1099-1646(199901/06)15:1/3<125::AID-RRR523>3.0.CO;2-E

Ward, J. V., Tockner, K., Arscott, D. B., & Claret, C. (2002). Riverine landscape diversity. *Freshwater Biology*, *47*(4), 517–539.

White, M. J., Arnold, J. G., Bieger, K., Allen, P. M., Gao, J., Čerkasova, N., Gambone, M., Park, S., Bosch, D. D., Yen, H., & Osorio, J. M. (2022). Development of a field scale SWAT+ modeling framework for the contiguous U.S. *JAWRA Journal of the American Water Resources Association*, *58*, 1545–1560. https://doi.org/10.1111/1752-1688.13056

Woessner, W. W. (2000). Stream and fluvial plain ground water interactions: Rescaling hydrogeologic thought. *Groundwater*, *38*(3), 423–429. https://doi.org/10.1111/j.1745-6584.2000.tb00228.x

Wohl, E. (2021). An integrative conceptualization of floodplain storage. *Reviews of Geophysics*, *59*(2), e2020RG000724. https://doi.org/10.1029/2020RG000724

Wohl, E., & Beckman, N. D. (2014). Leaky rivers: Implications of the loss of longitudinal fluvial disconnectivity in headwater streams. *Geomorphology*, *205*, 27–35. https://doi.org/10.1016/j.geomorph.2011.10.022

Wohl, E., Dwire, K., Sutfin, N., Polvi, L., & Bazan, R. (2012). Mechanisms of carbon storage in mountainous headwater rivers. *Nature Communications*, *3*(1), 1. https://doi.org/10.1038/ncomms2274

Wohl, E., Lininger, K. B., & Scott, D. N. (2017). River beads as a conceptual framework for building carbon storage and resilience to extreme climate events into river management. *Biogeochemistry*, *141*(3), 365–383. https://doi.org/10.1007/s10533-017-0397-7

Wohl, E., Rathburn, S., Dunn, S., Iskin, E., Katz, A., Marshall, A., Means-Brous, M., Scamardo, J., Triantafillou, S., & Uno, H. (2024). Geomorphic context in process-based river restoration. *River Research & Apps*, *40*, 322–340. https://doi.org/10.1002/rra.4236

Yan, L., & Roy, D. P. (2016). Conterminous United States crop field size quantification from multi-temporal Landsat data. *Remote Sensing of Environment*, *172*, 67–86. https://doi.org/10.1016/j.rse.2015.10.034

SUPPORTING INFORMATION

Additional supporting information can be found online in the Supporting Information section at the end of this article.

How to cite this article: Schulz, E. Y., Morrison, R. R., Bailey, R. T., Raffae, M., Arnold, J. G., & White, M. J. (2024). River corridor beads are important areas of floodplain-groundwater exchange within the Colorado River headwaters watershed. *Hydrological Processes*, *38*(9), e15282. https://doi.org/10.1002/hyp.15282